A Topology-Based Method for the Compartmentalization of Multiphysics Flows

by

Thomas Richard Donnelly

A thesis
presented to the University of Waterloo
in fulfillment of the
thesis requirement for the degree of
Master of Applied Science
in
Chemical Engineering (Water)

Waterloo, Ontario, Canada, 2020

Author's Declaration

This thesis consists of material all of which I authored or co-authored: see Statement of Contributions included in the thesis. This is a true copy of the thesis, including any required final revisions, as accepted by my examiners.

I understand that my thesis may be made electronically available to the public.

Statement of Contribution

This thesis contains work done using geometry and mesh files, to which I have made major contributions, originated by Dr. Tanyakarn Treeratanaphitak. Chapter 5 and Chapter 6 contain visualizations and descriptions of this geometry and mesh whose creation are attributable to Dr. Treeratanaphitak.

All other work in this thesis was performed by myself under the supervision of Professor Nasser Mohieddin Abukhdeir and Professor Mark Pritzker.

Abstract

Continuum simulations of multiphysics processes are costly due to the coupling of transport phenomena. Compartment modelling decouples hydrodynamics from other transport phenomena, offering a low-cost simulation alternative for applications such as design screening. While different methods will produce compartment models with different accuracy levels, no rigorous compartmentalization approaches currently exist.

In this work, a compartmentalization algorithm is proposed that identifies distinct flow modes from an analysis of the topology of a fluid velocity field. This topological analysis is based on an analogy between modes of fluid flow and deformation modes that have been identified for the molecular alignment of liquid crystals. A velocity alignment vector is defined and used to compute the deformation modes splay, twist, and bend for a velocity field.

This topologically-informed compartmentalization algorithm is developed through its application to a test case of steady single-phase laminar flow through a cylindrical vessel with a step increase in cross-sectional area. This case is observed to exhibit unidirectional, recirculatory, and diverging flow based on a continuum simulation. Local alignment deformation, defined as the sum of splay, twist, and bend for a velocity field, is computed and thresholded to segment the domain into compartments dominated by each of the distinct flow modes. These compartments are incorporated into a compartment model, which is validated against the continuum simulation through a comparison of their residence time distributions (RTDs). The compartment model RTD is shown to deviate from the continuum simulation in terms of having lower mean residence time, higher variance, and higher skewness.

The deviation between the compartment model and continuum simulation is attributed to the approximation of unidirectional compartments as well-mixed. The compartment model is modified to approximate each unidirectional compartment as a series of ideal continuous stirred-tank reactors (CSTRs), which improves the variance and skewness of the RTD but does not increase the mean residence time. As a final modification to the compartment model considered, an adjustment to the thresholding used for the compartment model is shown to have an insignificant effect on the RTD.

While additional work is required to improve the accuracy of the compartment modelling approach proposed, compartment models based on velocity topology offer a promising approach for multiphysics simulation.

Acknowledgements

I thank my supervisors, Professor Nasser Mohieddin Abukhdier and Professor Mark Pritzker, for their mentorship, guidance, and support through this project. I also thank Dr. Tanyakarn Treeratanaphitak for her input and assistance.

Additional thanks to the other members of the COMPHYS group for helping to maintain a sense of community (even when stuck working from home during a pandemic). Specific thanks to Alex Vasile, James Lowman, and Kimia Entezari as fantastic office mates and comrades in arms on this journey.

Thank you to Shannon, who has been an amazing partner through all of the ups and the downs. Thank you to Mango, Ramiro, Sheyla, and Triscuit for helping me always make time for walks.

I acknowledge and thank the following sources of funding: the University of Waterloo Engineering Excellence Fellowship, the Natural Sciences and Engineering Research Council of Canada (NSERC) Canada Graduate Scholarship Master's Program (CGS-M), the Ontario Graduate Scholarship (OGS) Program, and the RBC Water Scholars Graduate Entrance Scholarship. This funding supported me through the completion of this research.

Finally, I thank Compute Canada for the use of their computational resources.

The University of Waterloo is on lands that are deeply connected to Indigenous peoples who have historically lived and who currently live in this territory. These groups include the Neutral, Anishinaabeg, and Haudenosaunee peoples. The University of Waterloo is situated on the Haldimand Tract, the land promised to the Six Nations, also known as the Haudenosaunee people. This land includes six miles on each side of the Grand River.

Dedication

To my dad. Thanks for everything.

Table of Contents

List of Tables x

List of Figures xi

1 Introduction 1

1.1 Motivation . . . 1
1.2 Objectives . . . 3
1.3 Organization and Structure . . . 4

2 Background 6

2.1 Ideal Continuous-Flow Reactor Models . . . 6
2.2 Residence Time Distribution Analysis . . . 9
2.2.1 Determination of Residence Time Distribution . . . 9
2.2.2 Quantitative Description of Residence Time Distribution . . . 11
2.2.3 Residence Time Distribution for Ideal Reactors . . . 12
2.3 Compartment Modelling . . . 13
2.3.1 Comparison of Systemic, Continuum, and Compartment Modelling 13
2.3.2 Compartment Modelling Workflow . . . 15
2.3.3 Compartment Network Model . . . 17
2.3.4 Flows between Compartments . . . 18
2.3.5 Criteria for Compartmentalization . . . 18

3 Literature Review **20**

3.1 Review of Compartment Modelling Literature 20

3.1.1 History and Applications of Compartment Modelling 20

3.1.2 Existing Compartmentalization Methods 23

3.1.3 Problems with Existing Compartmentalization Methods 23

3.2 Review of Topological Analysis of Fluid Flow 25

4 Method: Topological Compartmentalization Approach **27**

4.1 Velocity Field Topology 27

4.2 Computation of Velocity Topology 29

4.3 Determining Compartments using Velocity Topology 31

5 Development of Topological Compartmentalization Algorithm **33**

5.1 Test Case: Cylindrical Vessel with Varying Cross-section 33

5.2 Consideration of Fluid Quantities 36

5.2.1 Velocity Magnitude 37

5.2.2 Vorticity 37

5.2.3 Velocity Gradient 38

5.3 Analysis of Fluid Alignment Vector 39

5.4 Analysis of Vector Topology Quantities 40

5.5 Analysis of Local Alignment Deformation 41

6 Application and Validation of Topological Compartmentalization Algorithm **43**

6.1 Initial Compartmentalization 44

6.2 Residence Time Distribution Comparison 46

6.2.1 Residence Time Distribution Computation for Continuum Simulation 47

6.2.2 Residence Time Distribution Computation for Compartment Model 47

6.2.3 Residence Time Distribution Comparison 49

6.3 Modelling Unidirectional Compartments as a Series of CSTRs 51
6.4 Variation of Compartmentalization Thresholding 53
6.5 Computation Time Comparison 55

7 Conclusions and Future Work **57**
7.1 Conclusions 57
7.2 Future Work 58

References **60**

List of Tables

2.1 Summary of comparison between systemic, compartment, and continuum modelling approaches. 13

6.1 Comparison of moments of RTDs for continuum solution and compartment model. 49

6.2 Comparison of RTD moments for continuum solution and compartment model with unidirectional compartments approximated as a series of CSTRs. 53

6.3 Comparison of computation times for obtaining RTDs for continuum solution and compartment models. 56

List of Figures

1.1 Example compartment model (right) to approximate convective and turbulent transport from a continuum simulation (left) for a stirred reactor. Obtained from [1]. 3

2.1 Diagrams of CSTR (left) and PFR (right). Obtained from [2]. 7

2.2 Illustration of modelling a PFR (top) with 5 CSTRs in series (bottom). Obtained from [2]. 8

2.3 Example residence time distribution plot. Obtained from [2]. 10

2.4 Concentration profiles obtained during tracer experiments at the inlet (left) and outlet (right) for pulse injection (top) and step injection (bottom) methods. Obtained from [2]. 10

2.5 Examples of a) systemic modelling of a dissolved air flotation tank (obtained from [6]) and b) continuum modelling solution for the velocity field of a stirred tank (obtained from [7]). 14

2.6 Illustration of mapping continuum grid (left) into compartmental network (right). Obtained from [3]. 15

2.7 Flow chart of compartment modeling procedure 16

2.8 Directionality of convective and turbulent flows between compartments. Obtained from [4]. 19

3.1 General classes of compartmentalization methods: left, aggregation of continuum elements into compartments, and right, division of system domain into compartments. Obtained from [4]. 24

3.2 Example of iterative compartmentalization process that divides the domain volume based on some quantity P. Obtained from [4]. 24

3.3 Different types of critical points for 2D flow. Obtained from [32]. 26

4.1 Examples of flow modes: (a) flow through a pipe, (b) contracting flow through a converging channel, and (c) recirculating flow seen in the vortices that develop in flow around a cylinder. Each obtained from [33]. . . . 28

4.2 Liquid crystal alignment modes: equilibrium (a) and deformation modes splay, twist, and bend (b), (c), and (d). Obtained from [34]. 29

4.3 Left: orientation of a liquid crystal molecule. Right: molecular alignment vector $\boldsymbol{n}$ representing average orientation of a group of molecules. Obtained from [36]. 30

4.4 Flow chart highlighting areas where topological compartmentalization deviates from existing compartment modeling procedure. 31

5.1 Geometry of test case used for investigation of topological compartmentalziation. 34

5.2 Mesh for case geometry visualized with cross-section in XY-plane (left) and through the centre of the case in the XZ-plane (right). 35

5.3 Visualization of velocity streamlines and velocity magnitude through the test case. 36

5.4 Visualization of velocity magnitude ($\sqrt{\boldsymbol{v} \cdot \boldsymbol{v}}$) through the test case. 37

5.5 Visualization of the magnitude of vorticity ($\boldsymbol{\nabla} \times \boldsymbol{v}$) through the test case. . 38

5.6 Visualization of the magnitude of the velocity gradient ($\boldsymbol{\nabla v}$) through the test case. 38

5.7 Visualization of the curl of the velocity alignment vector ($\boldsymbol{\nabla} \times \boldsymbol{n_v}$) through the test case. 39

5.8 Visualization of splay $(\boldsymbol{\nabla} \cdot \boldsymbol{n_v})^2$ through the test case. 40

5.9 Visualization of bend $(\boldsymbol{n} \times \boldsymbol{\nabla} \times \boldsymbol{n})^2$ through the test case. 41

5.10 Visualization of local alignment deformation through the test case. 41

6.1 Thresholding of local alignment deformation over velocity streamlines: Red for $f_f > 100$, green for $1 < f_f < 100$, and blue for $f_f < 1$. 44

6.2 Visualization of compartments resulting from compartmentalization 1. Plot of local alignment deformation over the test case (top) and resulting compartments used for the initial compartment model (bottom). The compartments are identified as follows: orange - inlet, green - outlet, purple - splay, red - recirculation, blue - stagnation zone. 45

6.3 Time profile of passive scalar T across the outlet from simulated tracer experiment for continuum solution. 48

6.4 Comparison of RTDs for continuum solution and compartment model with RTDs for idealized PFR and CSTR as reference. 50

6.5 Comparison of residence time distributions (RTDs) for continuum solution and compartment model. The number of CSTRs-in-series used to model flow through the inlet and outlet compartments is varied from 1 to 4. . . . 53

6.6 Visualization of compartments resulting from compartmentalization 2. . . . 54

6.7 Comparison of RTDs for continuum solution and compartment models generated with developed with different compartmentalization thresholds. . . . 55

Chapter 1

Introduction

1.1 Motivation

Multiphysics flows are characterized by the coupled transport of mass, momentum, and energy in the presence of fluid flow. Chemical engineering processes frequently involve simultaneous convective and diffusive transport of mass, momentum, and energy, as well as physical and chemical transformations. Additionally, these phenomena commonly occur across multiple interacting phases (i.e. multiphase flows). The timescale for convective transport is frequently much smaller than the timescales of other transport processes, particularly diffusion and many reactions (though this is not always the case, such as with gas diffusion or very fast reactions). However, to improve the performance of a process, engineers are often interested in understanding the effects of transport processes with longer timescales.

To model multiphysics processes, an important consideration is how to approximate the coupling of transport phenomena. In the simplest cases, this coupling is one-way, where fluid hydrodynamics are not significantly affected by composition, temperature, interactions with other phases, or other phenomena. As an approximation, equations for the conservation of mass and momentum of the fluid can be solved to obtain velocity and pressure fields, which can then be treated as "psuedo" steady-state on the time scale of other, slower phenomena. Other conservation equations can then be solved using the known velocity and pressure fields. In cases of two-way coupling, the velocity and pressure fields within a fluid are affected by other phenomena. For example, changes in fluid properties such as viscosity can change its velocity field. Fluid properties can be affected by temperature and composition, which can change due to mass and energy transport. Another example

is crystallization within a fluidized bed: as crystallization occurs, the size distribution of solid particles changes, which affects the fluid flow through the reactor. Two-way coupling presents a major computational challenge because simulation timesteps are limited by the timescale of the fastest process. Because of this challenge, the approximation of one-way coupling is frequently utilized.

In early stages of the design process, it is often necessary to simulate many design configurations to screen out designs that do not meet various objectives or constraints. Depending on the number of design candidates, it may not be feasible to carry out multiphysics simulations without making some simplifying assumptions. A trade-off exists between increasing simulation accuracy and reducing computational costs. During design screening, the highest accuracy is usually not necessary, so the multiphysics phenomena can be decoupled to reduce computational costs.

One approach to decoupling multiphysics phenomena is compartment modelling. This approach approximates a system as a network of interconnected compartments. The hydrodynamics of each compartment are approximated with a simple model, such as approximating compartments as ideally-mixed. The hydrodynamics of the system as a whole is approximated by constant fluxes between compartments, which are obtained based on the velocity field of an initial continuum simulation. These approximations decouple convection from other transport processes. After identifying compartments, the compartment network is modelled over a longer timescale to observe the effects of the other transport phenomena.

An example of a compartment model formulation is shown in Figure 1.1. In this example, a compartment model of a stirred-tank reactor is constructed based on the velocity field and turbulent dissipation energy ϵ from a Reynolds-averaged Navier Stokes (RANS) model simulation run using a $k - \epsilon$ turbulence closure. The range of ϵ is thresholded to create distinct compartments, and the velocity field is used to determine the fluxes between compartments, represented as arrows to indicate their direction and relative size.

The development of the network in a compartment model, also known as compartmentalization, frequently relies on the use of *ad hoc* heuristics. Compartments are often identified based on secondary mixing characteristics, such as variations in temperature or composition, rather than the mixing itself (*i.e.* the features of the velocity field). Variations in compartmentalization choices will ultimately affect the accuracy of the compartment model. Therefore, to improve the accuracy of the resulting modelling, it is necessary to develop well-justified principles for compartmentalization.

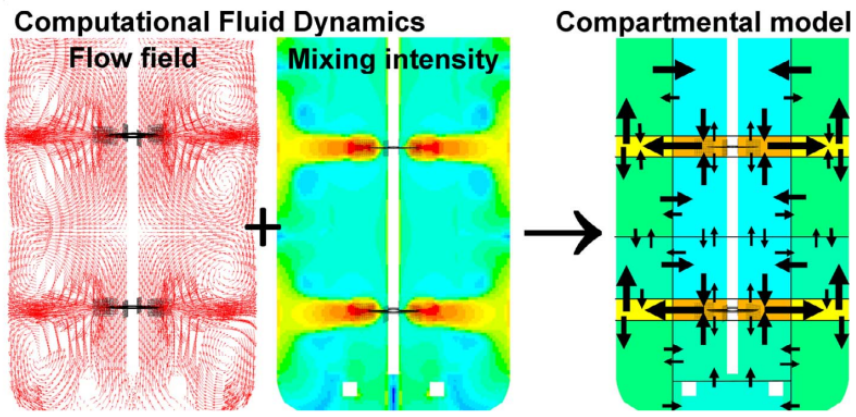

Figure 1.1: Example compartment model (right) to approximate convective and turbulent transport from a continuum simulation (left) for a stirred reactor. Obtained from [1].

1.2 Objectives

The overall objective of this work is to develop a method for compartmentalization based the fluid flow's *topology*, specifically the topology of the fluid velocity field. This topology-based compartmentalization will identify compartments with distinct flow behaviour. The distinctions in flow behaviour can be used to select the most appropriate hydrodynamic approximation for each compartment. Topology-based compartment modelling is intended to be used for design screening of multiphysics chemical engineering systems in which convective transport has a much smaller timescale than other transport phenomena.

The specific objectives of this work are as follows:

- Demonstrate how topological quantities representing modes of alignment deformation can be used to identify distinct modes of fluid flow.
- Propose a method for compartmentalization based on these topological quantities.
- Validate the proposed method based on its accuracy in replicating the residence time distribution (RTD) from a reference continuum solution. The reference solution will be obtained from a numerical solution of the Navier-Stokes equations for steady single-phase laminar flow.

1.3 Organization and Structure

This thesis is organized into seven chapters: Chapter 1 - Introduction, Chapter 2 - Background, Chapter 3 - Literature Review, Chapter 4 - Method: Topological Compartmentalization Approach, Chapter 5 - Development of Topological Compartmentalization Algorithm, Chapter 6 - Application and Validation of Topological Compartmentalization Algorithm, and Chapter 7 - Conclusions and Future Work.

Chapter 2 explains the background knowledge required to understand this work. Ideal reactor models for continuous flow systems are introduced and the relationship between modelling a series of continuous stirred-tank reactors and a single plug flow reactor is highlighted. Following this, the analysis of RTD is discussed, including determination of RTD by experiment or simulation and quantitative characterization of RTDs. Finally, an overview of compartment modelling is presented that covers the process of performing an initial continuum simulation, compartmentalization, and developing a network of compartments.

Chapter 3 presents a literature review summarizing the development and applications of compartment modelling and current compartmentalization approaches. A discussion is included on the challenges of the current state-of-the-art, specifically the lack of rigor in identifying the variables used for compartmentalization, the determination of thresholding levels for these variables, and automating this procedure. A brief review of visualization methods for fluid flow is included to introduce the concepts of topological analysis for fluid flow such as the identification of critical points in a velocity field.

Chapter 4 introduces the topological quantities that will be used for compartmentalization in this work. An analogy is drawn between different modes of flow and the modes of deformation of molecular alignment studied in liquid crystal physics. The velocity alignment vector is defined, which is used to compute topological quantities for fluid flow.

Chapter 5 introduces a test case with distinct flow modes for compartmentalization. Topological quantities are computed and observed to effectively capture the distinct flow modes. Local alignment deformation is computed as the sum of splay, twist, and bend for the test case, and thresholds are set for compartmentalization of the test case by this quantity.

Chapter 6 develops a compartment model based on the topological compartmentalization developed in Chapter 5. The compartment model is validated against the reference continuum simulation by comparison of RTD. The compartment model is modified by approximating unidirectional compartments as a series of CSTRs and by adjusting the

thresholds of local alignment deformation set for compartmentalization. With either modification, significant deviation between the RTDs remains. RTD computation times for the compartment model and continuum solution are compared.

Finally, Chapter 7 summarizes the conclusions of this work and provides recommendations for future work.

Chapter 2

Background

This chapter summarizes the background knowledge required to understand compartment modelling. First, a brief background on ideal models for continuous-flow reactors is presented, which is necessary for understanding the balances used for compartments in this work and in other compartment modelling work. Next, background is provided on residence time distribution, which is a common approach used to characterize mixing in non-ideal flow systems and will be used in this work to validate the proposed topology-based method for compartmentalization. Finally, background on compartment modelling is provided, which compares the modelling approach to conventional systemic and continuum modelling and explains the overall compartment modelling process.

2.1 Ideal Continuous-Flow Reactor Models

The understanding and application of ideal reactor models is foundational to reactor design and chemical reaction engineering [2]. In compartment modelling, ideal reactor models are used to approximate the hydrodynamics of compartments. This section provides relevant background on the ideal reactor models used in this work.

Two common configurations for industrial reactors are the continuous-stirred tank reactor (CSTR), primarily used for liquid-phase reactions, and the tubular reactor, primarily used for gas-phase reactions [2]. Diagrams to illustrate the ideal reactor models for these configurations are included in Figure 2.1. Ideal models for each system are developed by applying a general mole balance to the system and simplifying the balance with assumptions about mixing and flow characteristics.

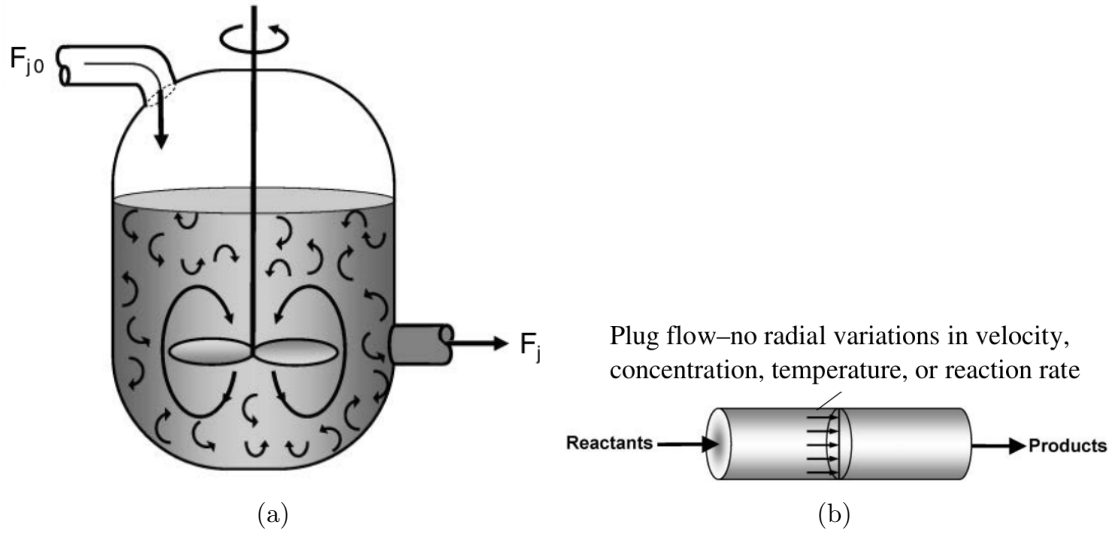

(a) (b)

Figure 2.1: Diagrams of CSTR (left) and PFR (right). Obtained from [2].

The ideal CSTR is assumed to be well-mixed, meaning that no variations exist in variables such as temperature, species concentration, or reaction rate inside the reactor, including at the reactor outlet. Under this assumption, for a single inlet and single outlet, the general mole balance for species j in a CSTR is as follows [2]:

$$F_{j,in} - F_{j,out} + r_j V = \frac{dN_j}{dt} \tag{2.1}$$

where $F_{j,in}$ and $F_{j,out}$ are the molar flow rates of j in and out of the system, r_j is the rate of production of j through chemical reaction, V is the volume of the reactor, and N_j is the total number of moles of j in the system. It is also commonly assumed that a CSTR operates at steady-state, which eliminates the time derivative on the right hand side of the equation, however this cannot be done for operation periods such as startup that are inherently transient.

For homogeneous (i.e. single-phase) reactions, the flow through an ideal tubular reactor is assumed to be plug-flow, meaning that the fluid velocity profile within the reactor has no variations in the radial direction. A plug-flow tubular reactor is conventionally referred to as a plug-flow reactor (PFR). Because variations will exist in the axial direction of a PFR, steady-state conditions are usually assumed to simplify the mole balance. If this assumption is not made, the model of a PFR takes the form of a partial differential equation due to derivatives in space and time.

The mole balance for species j in a steady-state PFR is as follows [2]:

$$\frac{dF_j}{dV} = r_j \tag{2.2}$$

The behaviour of a PFR can be approximated by a cascade of CSTRs in series. This approximation is useful for simplifying the PFR mole balance in situations where steady-state conditions cannot be assumed, such as modelling catalyst decay in packed-bed reactors or transient heat effects in PFRs [2]. The relationship between the volume of a PFR and the volume of each CSTR in the cascade in this approximation is as follows:

$$V_{CSTR} = \frac{V_{PFR}}{n_{CSTR}} \tag{2.3}$$

where V_{PFR} is the volume of the PFR being approximated, V_{CSTR} is the volume of each CSTR in the series, and n_{CSTR} is the number of CSTRs in the series. This is shown with an example of 5 CSTRs in series in Figure 2.2. This approximation is mathematically equivalent to applying a general mole balance to a PFR, discretizing the axial spatial dimension with an even spacing, and solving the resulting equation numerically with a zero-order interpolating function.

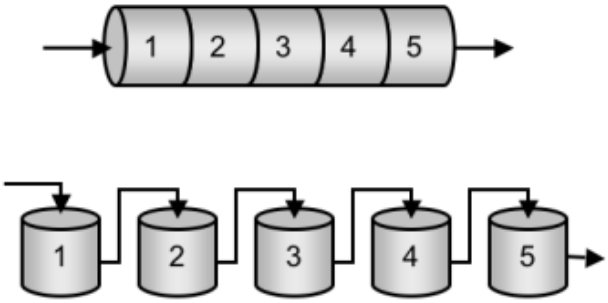

Figure 2.2: Illustration of modelling a PFR (top) with 5 CSTRs in series (bottom). Obtained from [2].

Assuming perfect mixing and transient operation, a general mole balance for a series of CSTRs can be obtained from Equations 2.1 and 2.3:

$$\frac{dN_{j,1}}{dt} = F_{j,in} - F_{j,1\to 2} + r_{j,1}V \tag{2.4}$$

$$\frac{dN_{j,\alpha}}{dt} = F_{j,\alpha-1\to\alpha} - F_{j,\alpha\to\alpha+1} + r_{j,\alpha}V \quad \text{for} \quad 1 < \alpha < n_{CSTR} \tag{2.5}$$

$$\frac{dN_{j,n_{CSTR}}}{dt} = F_{j,n_{CSTR}-1\to n_{CSTR}} - F_{j,out} + r_{j,n_{CSTR}}V \tag{2.6}$$

where α identifies the CSTRs from 1 (the CSTR at the PFR inlet) to n_{CSTR} (the CSTR at the PFR outlet).

2.2 Residence Time Distribution Analysis

Residence time distribution (RTD) analysis will be used in Chapter 6 to quantitatively validate the topological compartmentalization approach developed in Chapter 5. RTD analysis is a common approach for characterizing mixing within the system. The amount of time that elapses between material entering and leaving a system is known as residence time. Residence time is quantified as a distribution because proportions of material that enter will remain in the reactor for different durations before being discharged. An example residence time distribution is plotted in Figure 2.3. The residence time distribution function is conventionally denoted as $E(t)$, with units of inverse time such as s^{-1}. The percent of material that flows through the system with a residence time between t_1 and t_2 is obtained by taking the integral $\int_{t_1}^{t_2} E(t)dt$.

2.2.1 Determination of Residence Time Distribution

The RTD has traditionally been determined experimentally through tracer experiments [2, 3, 4]. In tracer experiments, an inert species is injected at the inlet of a system and its concentration is measured at the outlet. The concentration measurement at the outlet is plotted and analyzed to obtain a RTD. The most common injection methods are the pulse input and step input. For a pulse input, a fixed amount of tracer is injected at a single time, so the inlet concentration profile approximates a Dirac-delta function. For a step input, once the injection begins, the amount of tracer introduced into the system remains constant over time, so the inlet concentration profile approximates a step function. Characteristic tracer concentration profiles for each injection method at the inlet and outlet of a system are shown in Figure 2.4.

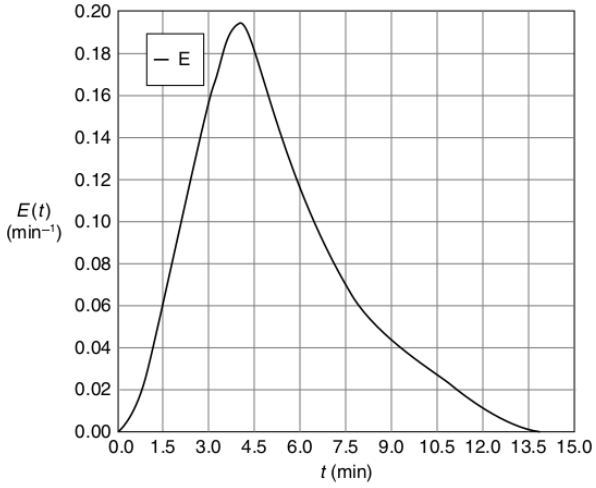

Figure 2.3: Example residence time distribution plot. Obtained from [2].

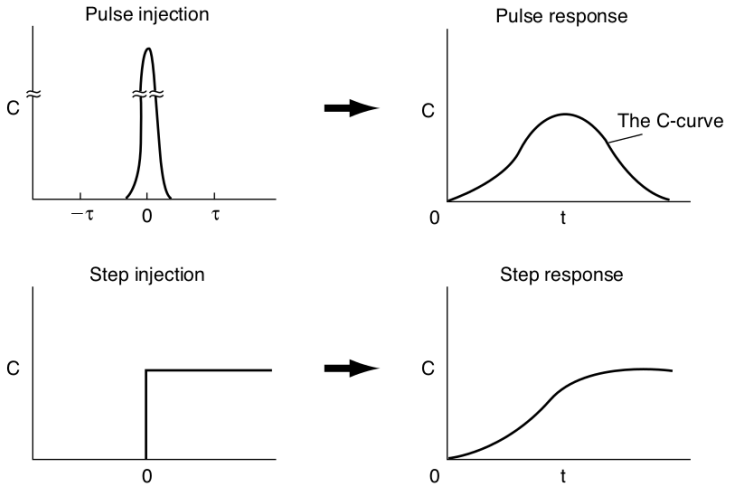

Figure 2.4: Concentration profiles obtained during tracer experiments at the inlet (left) and outlet (right) for pulse injection (top) and step injection (bottom) methods. Obtained from [2].

The RTD function $E(t)$ can be computed for a pulse input injection as [2]:

$$E_{pulse}(t) = \frac{QC_{out}(t)}{N_0} \tag{2.7}$$

where Q is the outlet volumetric flowrate, $C_{out}(t)$ is the concentration of the tracer at the outlet, and N_0 is the total number of moles of tracer that was injected in the pulse.

For a step input injection, the RTD function is computed as [2]:

$$E_{step}(t) = \frac{d}{dt}\left(\frac{C_{out}(t)}{C_0}\right) \tag{2.8}$$

where C_0 is the concentration of tracer that is maintained in the injection at the inlet.

The RTD of a system can also be obtained by simulating the transport of a passive scalar over a steady-state velocity field. Numerically, a passive scalar is simply a dimensionless scalar field that is conserved and advected with the flow using a complete convection-diffusion equation. With a constant diffusion coefficient[1], this equation is [5]:

$$\frac{\partial T}{\partial t} + \boldsymbol{\nabla} \cdot (\boldsymbol{v}T) - \boldsymbol{\nabla}^2 (D_T T) = 0 \tag{2.9}$$

where T is the value of the passive scalar, $\boldsymbol{v}$ is the fluid velocity field, and D_T is the diffusion coefficient divided by the fluid density. As with an experimental tracer, the passive scalar does not affect the fluid flow, and is simply transported along with the bulk flow. Therefore, the dimensionless concentration of a species that does not participate in reactions or affect the fluid properties is an example of a passive scalar. D_T is set to 0 so that the passive scalar is only convected, meaning the passive scalar only follows the fluid velocity field.

The passive scalar value T is substituted for concentration in Equations 2.7 or 2.8 to obtain the residence time distribution from a pulse or step injection simulation.

2.2.2 Quantitative Description of Residence Time Distribution

Since RTDs are distribution functions, they can be described and compared quantitatively by their moments [2]. The mean residence time t_m is the first moment of the RTD function $E(t)$, which is the average amount of time that material spends within the system:

$$t_m = \int_0^\infty tE(t)dt \tag{2.10}$$

[1] In the most general convection-diffusion equation, the diffusion term is $\boldsymbol{\nabla} \cdot (D_T \boldsymbol{\nabla} T)$. With a constant diffusion coefficient, this term simplifies to $\boldsymbol{\nabla}^2 (D_T T)$. The approximation of constant diffusion coefficient is generally valid for experimental tracers, since the concentrations used in tracer experiments are very small; for transport of passive scalars, a constant diffusion coefficient is set by definition.

The second and third moments are also commonly used to characterize RTD functions. The calculations of these moments are centered at the mean residence time t_m. The variance σ^2 of $E(t)$ is calculated as the second moment, which indicates the spread of the distribution:

$$\sigma^2 = \int_0^\infty (t - t_m)^2 E(t) dt \tag{2.11}$$

The skewness s^3 of $E(t)$ is calculated as the third moment, which quantifies how skewed $E(t)$ is to one side of the mean:

$$s^3 = \int_0^\infty (t - t_m)^3 E(t) dt \tag{2.12}$$

The mean residence time t_m, variance σ^2, and skewness s^3 are generally sufficient to quantitatively characterize and compare RTDs [2].

2.2.3 Residence Time Distribution for Ideal Reactors

The residence time distributions for a single ideal CSTR and single ideal PFR are as follows [2]:

$$E_{CSTR}(t) = \frac{e^{\frac{-t}{\tau}}}{\tau} \tag{2.13}$$

and

$$E_{PFR}(t) = \delta(t - \tau) \tag{2.14}$$

where $\tau = V/Q$ is space time, defined as the ratio of system volume V to total volumetric flow rate Q, and δ is the Dirac-delta function.

2.3 Compartment Modelling

2.3.1 Comparison of Systemic, Continuum, and Compartment Modelling

This section will define and compare compartment modelling, systemic modelling, and continuum modelling. Each of these three modelling approaches formulates and solves a system of conservation balances for mass, momentum, energy, and any other conserved quantities of interest. The fundamental differences are in the approach for discretizing a system into the elements over which balances are formulated. These differences determine the complexity of the mathematical equations to be solved, the number of elements over which they must be solved, and the relative accuracy and computational requirements of obtaining a solution. A comparison of the three approaches is summarized in Table 2.1.

Table 2.1: Summary of comparison between systemic, compartment, and continuum modelling approaches.

	Systemic Modelling	Compartment Modelling	Continuum Modelling
System of Equations	Ordinary Differential (Unit Balances)	Ordinary Differential (Unit Balances)	Partial Differential (e.g. Navier-Stokes)
Typical Number of Elements	<10	$10 - 10^3$	$10^3 - 10^6$
Accuracy	Low	Moderate	High
Computation Time	Low	Moderate	High

Systemic modelling, also known as reduced order or reactor network modelling, describes a system as a network of ideal reactors, typically PFRs and CSTRs. Decisions about the type, number, and configuration of ideal reactors is generally based on an understanding of the global flow behaviour, often quantified using the RTD [2]. The RTD is traditionally determined experimentally through tracer experiments [2, 3, 4]. This approach typically uses less than 10 ideal reactors (or elements), and it formulates and applies conservation balances on each. By discretizing the spatial dimension of PFRs using the CSTR-in-series approximation discussed in Section 2.1, the fluid flow evolves only in time in the most general situation. Therefore, the system to be solved contains algebraic or ordinary differential equations and is relatively simple to solve. This is a black box approximation in that only input and output quantities are modelled and the details of flow

behaviour within the system are ignored. An example of the systemic approach used to model a dissolved air flotation tank is shown in Figure 2.5a.

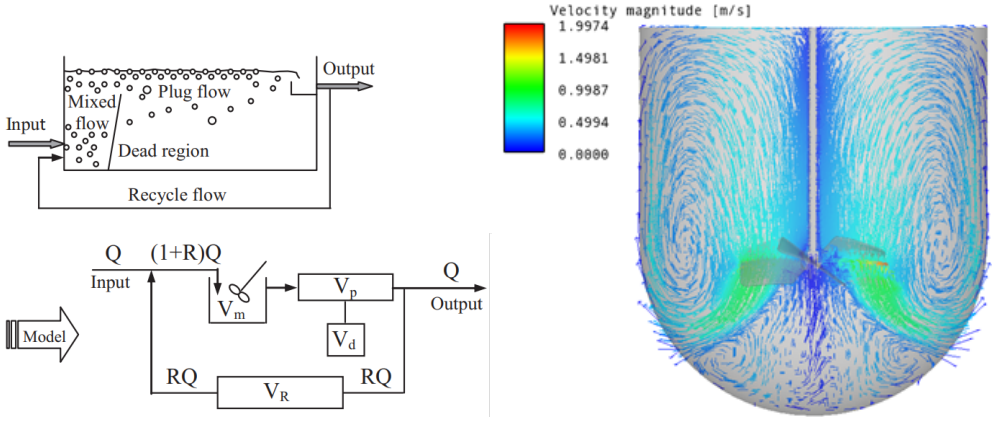

(a) (b)

Figure 2.5: Examples of a) systemic modelling of a dissolved air flotation tank (obtained from [6]) and b) continuum modelling solution for the velocity field of a stirred tank (obtained from [7]).

Continuum modelling, in contrast, formulates and numerically solves conservation balances for a system by discretizing a domain along spatial dimensions. Since flow behaviour can evolve over space and time, the system to be solved is a set of partial differential equations, such as the Navier-Stokes equations. Decisions regarding the discretization of the geometry are often left to the user, but greatly affect simulation accuracy. Ideally, these decisions are made based on an understanding of the system geometry and expected flow behaviour (e.g. presence of baffles and impellers, expected flow profile, turbulent behaviour, etc). Depending on the system to be simulated and the desired level of accuracy, this process can generate very large numbers of elements. Simulations with millions of elements are common when high accuracy is required. This approach has the highest computational cost, but it will provide highly accurate solutions if balances are formulated, discretized, and solved using the most appropriate methods. An example flow profile obtained from the solution of a continuum model over a stirred tank is shown in Figure 2.5b.

Compartment modelling can be characterized as a hybrid approach between systemic and continuum modelling. In this approach, a network of compartments is developed by segmenting a domain based on the solution of a continuum simulation. While systemic modelling segments the domain based on RTD experiments, which only provide information about global flow behaviour, segmentation in compartment modelling is based on an

understanding of the physical system geometry and local flow characteristics [3]. Compartments are chosen to represent distinct flow regions; specifically, since compartments are usually assumed to be perfectly mixed, they are generally chosen to correspond to regions where important process variables are homogeneous. The continuum solution is then used to determine flows between the resulting compartments (see Figure 2.6). Since compartments are traditionally assumed to be well-mixed, which eliminates spatial gradients, compartment model conservation balances are generally either algebraic or ordinary differential equations. Compartment models are generally constructed with more elements than systemic models, but fewer than continuum models, with 10-1000 compartments being typical [4].

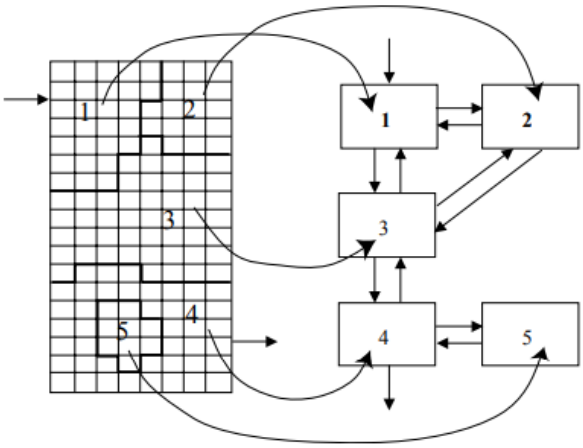

Figure 2.6: Illustration of mapping continuum grid (left) into compartmental network (right). Obtained from [3].

2.3.2 Compartment Modelling Workflow

The general workflow for developing and solving a compartment model can be summarized as follows (see Figure 2.7):

1. **Initial Continuum Simulation**: A continuum simulation is performed to obtain an initial profile for flow and other characteristics. The system is simulated over a limited time period, generally based on the convective timescale. Transport processes and transformations that are much slower (e.g. surface chemical reactions) can be neglected.

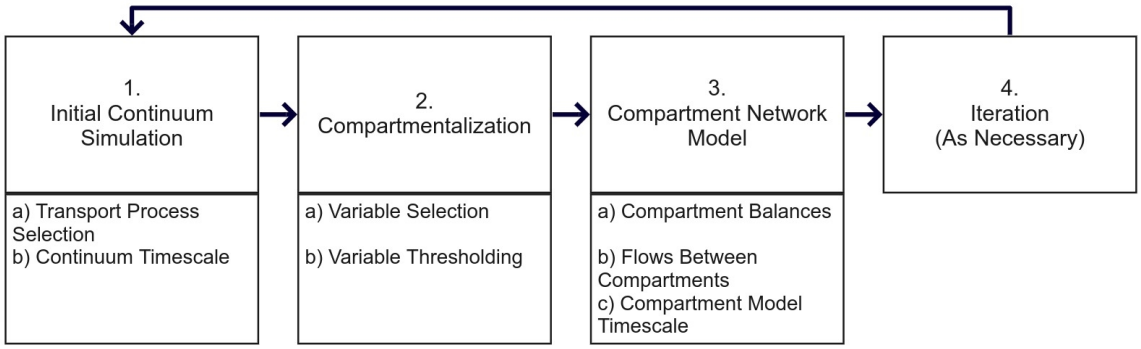

Figure 2.7: Flow chart of compartment modeling procedure

2. **Compartmentalization**: The resulting flow profile and other information is used to divide the physical space of the domain into compartments (see Figure 2.6). For the compartment model to be physical, the compartments must span the entire domain, and each compartment should be contiguous, meaning that no point is isolated from other points in the compartment. Additionally, material can only flow between adjacent compartments.

3. **Compartment Network Model**: Conservation balances are formulated for each compartment (see Section 2.3.3), and flow rates between the compartments are determined (see Section 2.3.4). Compartments are typically assumed to be perfectly mixed when formulating conservation balances.

4. **Iteration**: The first iteration loop is the iteration of the compartment model over time. Steps in this iteration loop are based on the timescale of the other transport phenomena or transformations of interest. The first loop is completed either when the user has simulated the longer time period of interest, or when the user suspects that the slower processes have occurred significantly enough to alter the flow profile of the system. In the latter case, the second iteration loop occurs, in which the user reruns the continuum simulation using the solution from the compartment model as an initial condition. After a new steady-state velocity field is obtained, the compartment model is redeveloped, and the first iteration loop repeated. The second iteration loop continues until the user has simulated the total time period of interest.

The predictions of a compartment model may be validated against references of ei-

ther a full continuum simulation or experimental data. Validation may be based on flow behaviour, such as residence time distributions, or process-specific quantities, such as concentration profiles. Section 3.1.1 discusses different data that have been previously used for validation. If the continuum simulation used for compartmentalization is valid, error in a compartment model results from either the compartmentalization (step 2) or the compartment network model (step 3).

2.3.3 Compartment Network Model

Once compartments have been identified as in Figure 2.6, it is necessary to develop conservation balances for mass, energy, and any other quantities of interest for each compartment (step 3 in Section 2.3.2). These conservation balances are developed by modelling each compartment as a simpler reactor, typically as a well-mixed CSTR. As an example, Equation 2.15 is a compartment mass balance for component k in compartment i in a single-phase system, treating compartment i as a single CSTR:

$$V_i \frac{dc_{k,i}}{dt} = \sum_{j=1}^{n_c} \left(Q_{j \to i} c_{k,j} - Q_{i \to j} c_{k,i} \right) + r_i V_i \tag{2.15}$$

where

- V_i is the volume of the ith compartment
- $c_{k,i}$ is the concentration of component k in the ith compartment (constant through the compartment since the compartment is assumed well-mixed)
- n_c is the number of compartments
- $Q_{j \to i}$ is the volumetric flow rate of material from compartment j to compartment i (note that this value is 0 if compartments j and i do not share an interface)
- r_i is the rate of formation of i due to chemical reaction.

Note that Equation 2.15 applies only to a compartment in the domain that does not include system inlets or outlets. Additional terms need to be included for compartments with flows entering or leaving the system.

2.3.4 Flows between Compartments

The flow $Q_{j\to i}$ between compartments must be determined before the compartment model can be solved. $Q_{j\to i}$ is determined as the sum of flow due to convective transport ($Q^C_{j\to i}$) and flow due to turbulent transport ($Q^T_{j\to i}$), as in Equation 2.16:

$$Q_{j\to i} = Q^{conv}_{j\to i} + Q^{turb}_{j\to i} \tag{2.16}$$

$Q^{conv}_{j\to i}$ can be determined simply by integrating the velocity field over the surface A_{ji} between the two compartments. The surface A_{ji} between two compartments[2] is defined such that the surface normal $\hat{n}$ always points from compartment j to compartment i. This integral is then calculated where the dot product of velocity and the surface normal is positive [8]:

$$Q^{conv}_{j\to i} = \iint_{A_{ji}} (\boldsymbol{v}\cdot\hat{n})\,dA \quad for \quad \boldsymbol{v}\cdot\hat{n} > 0 \tag{2.17}$$

Only areas where $\boldsymbol{v}\cdot\hat{n}$ is positive are included in the calculation of $Q^{conv}_{j\to i}$. Areas where this term is negative represent flow moving from compartment i to compartment j based on the definition of A_{ji}. Flows from compartment i to compartment j are included in the calculation of the term $Q_{i\to j}$ included in Equation 2.15. Calculating flows between compartments this way (as opposed to taking the net flow between compartments) is necessary since flows from compartment j have different properties (e.g. composition) than flows from compartment i.

While the convective flow term $Q^{conv}_{j\to i}$ is unidirectional, the turbulent flow term $Q^{turb}_{j\to i}$ is bidirectional because it results from turbulent mixing that occurs at the interface between the compartments. This is illustrated in Figure 2.8. Several ad-hoc approaches exist for calculating the turbulent flow term [4]. However, these are not a major interest for the purposes of this project; as such, turbulent flow terms will be neglected.

2.3.5 Criteria for Compartmentalization

To segment a domain into compartments (compartmentalization, Step 2 in Section 2.3.2), a variety of approaches exist. These approaches may be based on the system geometry, the

[2]This surface can have any shape depending on how the compartments are identified.

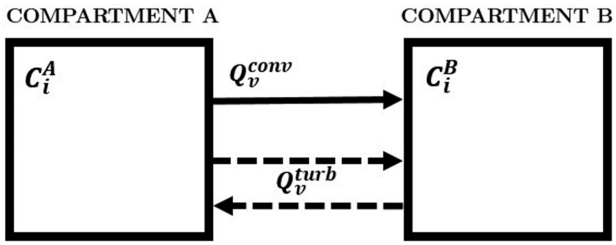

Figure 2.8: Directionality of convective and turbulent flows between compartments. Obtained from [4].

velocity field, or any other fields (e.g. concentration, rates of chemical reaction, etc) obtained from the initial continuum simulation (Step 1 in Section 2.3.2) [4]. The approaches for discretizing the domain into compartments based on thresholding any of these fields also vary. After identifying compartments, the compartment network may also be manually adjusted to avoid having excessively many compartments or compartments that are unnecessarily small. The lack of standardized methods for compartmentalization is a major challenge for compartment modelling. This lack of standardization is particularly problematic because these decisions will directly determine the accuracy of the compartment model. Existing compartmentalization approaches will be discussed in detail in Section 3.1.2.

Chapter 3

Literature Review

3.1 Review of Compartment Modelling Literature

The first goal of this chapter is to review the history of compartment modelling including its origin, mathematical generalization, and recent applications. Since compartment modelling was most clearly formalized in the mid 2000s, Section 3.1.1 will briefly cover research on compartment modelling from the 1990s to this period, as well as applications of compartment modelling in more recent years. The remainder of the literature review will specifically focus on current methods for compartmentalization and their limitations, as discussed in Section 3.1.2. Finally, Section 3.1.3 summarizes the limitations of current compartment modelling.

Another goal of this chapter is to identify the hydrodynamic models that have been used for approximating the flow in individual compartments. However, to the best of the author's knowledge, all previous work on compartment modelling has been based on the assumption that each compartment is well-mixed. This is in contrast to systemic modelling, in which PFR and other simple reactor models are commonly applied.

3.1.1 History and Applications of Compartment Modelling

Origins of Compartment Modelling

Early references to compartment modelling before the approach was formalized can be found from the 1990s through to the early 2000s. During that period, various terminol-

ogy was used for compartment modelling, including network-of-zones, multiblock, multizone/multizonal modelling, and compartmental modelling itself. The applications for these models include crystallizers [9, 10], activated sludge reactors for wastewater treatment [11], and suspension polymerization reactors [12]. Ref. [9] describes the compartmental approach as analogous to the stage-based approach used for modelling distillation columns. Compartments were generally identified heuristically based on the system geometry and expected flow behaviour [9, 12], although a modified approach in which adjustments were made to such compartments based on gradients in local energy dissipation determined from a $k - \epsilon$ continuum simulation has been reported [10]. Interestingly, compartmentalization based on the internal age distribution calculated throughout the system from a continuum simulation has also been reported [11]. The compartments were assumed to be well-mixed in each of these cases, which is an improvement over models that treat the whole system as well-mixed.

Formalization of Compartment Modelling

Several studies from the mid-2000s present general formulations for compartment modelling and are generally considered to be foundational. After applying compartment modelling to a non-Newtonian aerobic bioreactor [13], the authors later propose a framework for compartment modelling [14] as well as criteria and a method for automating compartmentalization [15]. In this framework, a user selects one or more variables for compartmentalization as well as a tolerance for each property. For example, the bioreactor is compartmentalized based on fluid viscosity, which varies as a function of shear stress. The authors then propose two compartmentalization approaches. The first compartmentalization approach selects a seed cell from the continuum simulation and aggregates neighbouring cells for which the properties selected are within the specified tolerances. The second approach separates regions of stagnant or recirculating flow before performing compartmentalization on each region individually. With both approaches, the authors suggest combining compartments below a certain size since the inclusion of such compartments does not significantly improve model accuracy. This framework treats the identified compartments as well-mixed.

Another general formulation for compartment modelling is presented in ref. [3], which applies this formulation to a bubble column. Compartmentalization in this work is performed manually based on heuristics and a qualitative analysis of the flow field.

Recent Applications of Compartment Modelling

Research involving compartment modelling since the mid-2000s has primarily focused on applications with few major deviations from the previously discussed general formulations. The majority of these studies apply compartment modelling to a stirred batch bioreactor [1, 16, 17, 18, 19]. Stirred batch bioreactors are a common application for compartment modelling due to the computational challenges of solving a continuum simulation that must capture the impeller movement, multiphase (gas-liquid) mass and momentum transfer, and chemical reactions/cell growth. Other stirred batch reactor applications have included batch cooled crystallizers [20, 21] and high shear granulation [22]. Compartment modelling has also been applied to continuous systems including a stirred autoclave for low-density polyethylene production [23], channel reactors for wastewater treatment [8, 24], a bubble column photobioreactor [25], and a waste stabilization pond [26].

While compartment models are often validated against the reference continuum simulations used for compartmentalization, validation against experimental data is also common. One approach for experimental validation is to compare the residence time distribution or concentration profile predicted by the compartment model against tracer experiments [8, 18, 17, 26]. Experimental validation has also been performed based on process-specific variables such as reactant gas concentration profiles [24], biomass concentration profiles [25], particle size distributions [19], bubble size distributions [22], oxygen transfer rates [19], and biomass growth rates [25].

Energy conversion, particularly gasification for syngas conversion, is another potential application for compartment modelling. It is difficult and impractical to incorporate full continuum models for entrained flow gasifiers (EFGs) into plant-scale models [27]. Ref. [27] developed a general reduced order model (ROM) consisting of a network of CSTRs and PFRs to simulate a range of existing gasifier and syngas cooler configurations. This general model has been modified and implemented for specific EFG configurations and operating conditions, such as for the Shell-Prenflo family of gasifiers [28]. Ref. [29] developed a similar model for the steady-state operation of a short-residence time EFG. The same authors expanded this model to predict transient performance of the short-residence time EFG [30]. Reactors in these ROMs were identified based on qualitative observations of flow behaviour from a continuum simulation. These ROMs are very similar to compartment models, though compartment networks have not traditionally incorporated PFRs.

3.1.2 Existing Compartmentalization Methods

Compartmentalization (Step 2 in Section 2.3.2) is a fundamental step of compartment modelling. The use of different compartmentalization methods will affect the number, size, and shape of compartments generated. This, in turn, will influence the accuracy of the compartment model. Therefore, it is important to understand existing methods for compartmentalization as well as their limitations.

Methods for compartmentalization of a continuum simulation result (Step 1 in Section 2.3.2) can be organized into two major classes, as shown in Figure 3.1. The first class is division of the entire volume: in this approach, the domain is divided into compartments based on some rules or heuristics (see Figure 3.2). This can be done automatically or manually, based on a user's judgement. The second class aggregates elements from the mesh used in the continuum simulation. In this approach, a variable and tolerance are selected for aggregation. Next, a mesh element is selected and combined with neighbouring elements that meet the selected tolerance criteria; this is repeated until all mesh elements have been grouped into a compartment. Because the number of elements in a continuum simulation is typically quite large (tens of thousands to millions), this approach is generally automated, although manual adjustments may be made to merge compartments that the user deems excessively small.

Compartmentalization methods can also be grouped based on the criteria for compartmentalization [4]. These criteria may include geometry, flow characteristics, or other process variables. Compartmentalization by flow characteristics for stirred batch reactors is commonly performed based on the axial and radial components of velocity [16, 17, 18, 20]. Other process variables are chosen for compartmentalization based on their importance in determining reaction rates or other transport phenomena. Other choices have included solid or gas phase fractions [22, 24], turbulence quantities such as mixing intensity [1, 24, 25], reactant concentrations [8], reaction rates [23], temperature [21, 23], and various combinations of these variables.

In addition to the many variables with which to perform compartmentalization, an even larger variety exists in the compartmentalization thresholds that are set. These choices are overwhelmingly heuristics-based.

3.1.3 Problems with Existing Compartmentalization Methods

A major problem with existing compartmentalization methods is the lack of standardization in their approach. Specifically:

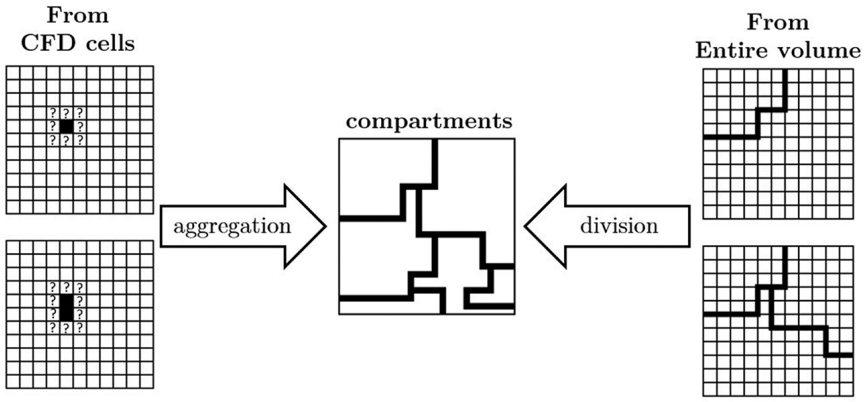

Figure 3.1: General classes of compartmentalization methods: left, aggregation of continuum elements into compartments, and right, division of system domain into compartments. Obtained from [4].

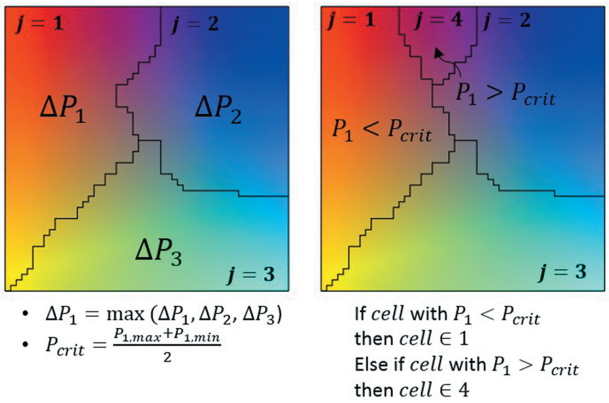

Figure 3.2: Example of iterative compartmentalization process that divides the domain volume based on some quantity P. Obtained from [4].

- **Variables for Compartmentalization**: Since no standard approach exists for selecting variables to use as the basis for segmentation, it is currently left to the user to use judgement on the variables that are important in a process (e.g. concentrations, mass transfer rates, reaction rates).

- **Thresholding of Variables**: Similarly, once a choice is made regarding the variables to be used for compartmentalization, no standard approach exists for thresholding the variables to identify different compartments.

- **Automation Tools**: The approaches for automation of compartmentalization in the literature vary, and often involve ad-hoc approaches to obtain a desired number of compartments and combine compartments which are deemed to be too small.

As previously noted, changes in the compartmentalization method will result in variation in model accuracy, and very little work in understanding this relationship has been reported. Ensuring the accuracy of compartment models motivates the development of a standardized, automated compartmentalization method based on universal flow quantities that could be applied to any reactor system.

3.2 Review of Topological Analysis of Fluid Flow

As discussed in Section 3.1.3, it is important to develop a standardized compartmentalization method based on universal flow quantities that could be applied to any system. Compartmentalization based on the velocity magnitude and its components has been previously used, but these approaches have been heuristics-based. Alternatively, a topologically-informed analysis of flow fields can be found in the field of flow visualization.

A review of geometry-based methods for the visualization of fluid flow is provided in ref. [31]. Such methods place discrete objects in the velocity field in order to reflect the underlying properties of the flow. These geometric objects include curves (i.e. streamlines), surfaces (i.e. stream surfaces), and volumes. Streamlines and stream surfaces are produced by integrating the velocity from an initial point or curve (selected by the user in a process referred to as seeding) to produce an object tangent to the velocity field at every point.

One consideration for fluid flow visualization is the presence of critical points. Critical points in a velocity field are locations where the magnitude of velocity is 0. Behaviour of the flow around a critical point can be used to classify the critical points. A method to visualize flow behaviour near critical points was developed in [32]. Critical points can be classified based on the types presented in Figure 3.3. For incompressible flow, the types of critical points relevant are centers of recirculation regions, and saddles, observed when flow from two opposing directions connect.

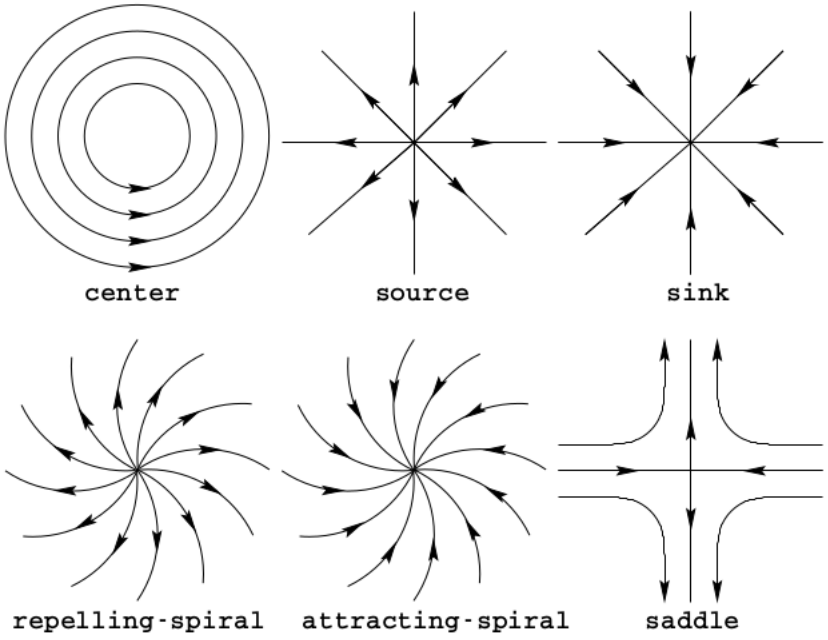

Figure 3.3: Different types of critical points for 2D flow. Obtained from [32].

Chapter 4

Method: Topological Compartmentalization Approach

The goal of this chapter is to introduce and justify the topological quantities that will be used for compartmentalization. First, a discussion of the topology of fluid velocity fields is provided to identify distinct modes of fluid flow. Parallels are drawn between these flow modes and modes of deformation observed in the molecular alignment of liquid crystals. Next, the computation of deformation quantities for liquid crystal molecular alignment is introduced. This computation is based on the molecular alignment vector $\boldsymbol{n}$; therefore, a corresponding velocity alignment vector $\boldsymbol{n_v}$ is defined so that these alignment deformation quantities can be computed for fluid velocity fields. Finally, an overview is given for the proposed topologically-informed compartmentalization approach. This approach will be explored in detail in Chapter 5.

4.1 Velocity Field Topology

Fluid flow through a domain will exhibit different behaviour depending on the geometry of the system. From observing this behaviour, it is possible to identify distinct modes of flow. These flow modes include unidirectional flow, such as that through a pipe or a duct; diverging or converging flow[1], such as that through a channel with varying cross-sectional area; twisting flow, such as that through a fan or other turbomachinery; recirculating

[1]Diverging and converging refer to the boundaries of the flow such as physical walls of a channel, rather than to the fluid itself. Incompressible flow always has a divergence of 0.

flow, such as the circulation patterns observed in a closed stirred tank; and stagnant flow. Examples of unidirectional, converging, and recirculatory flow are shown in Figure 4.1. Distinction between these flow modes is made based on the spatial dependence of the *direction* of the fluid velocity field, not its magnitude: for example, flow through a pipe is considered unidirectional whether its flow profile is parabolic (as in laminar flow) or uniform (as in plug flow).

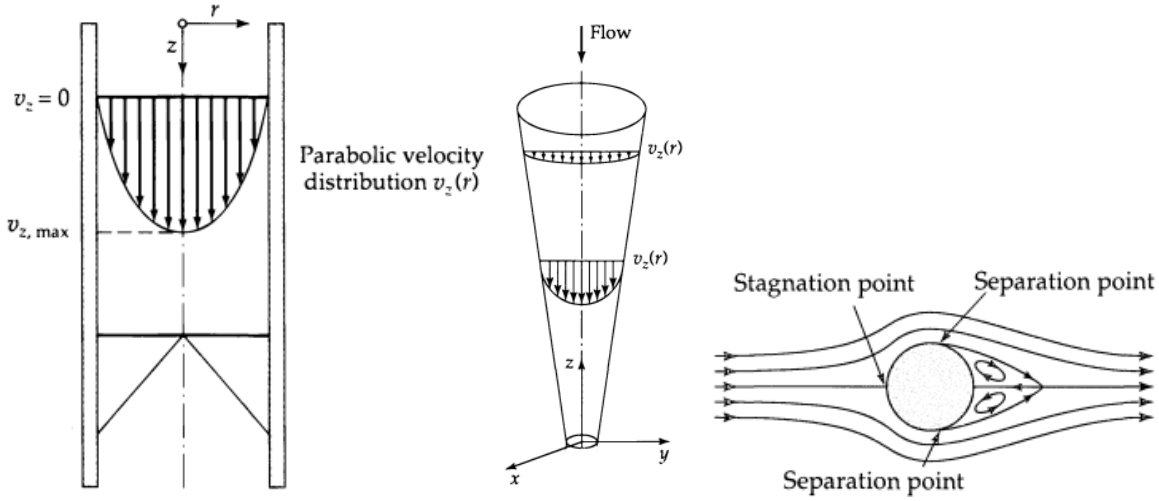

(a) (b) (c)

Figure 4.1: Examples of flow modes: (a) flow through a pipe, (b) contracting flow through a converging channel, and (c) recirculating flow seen in the vortices that develop in flow around a cylinder. Each obtained from [33].

An analogy can be made with the alignment of molecules in a liquid crystal phase. The molecular alignment of liquid crystals is studied because it determines physical properties of the phase. Molecular alignment can be classified based on its deviation from equilibrium alignment, where all molecules have the same orientation in space. Figure 4.2 shows a visualization of the equilibrium alignment as well as the independent modes of deformation known as splay, twist, and bend. By generalizing these modes of alignment to the alignment of other vector fields, unidirectional fluid flow would be the equilibrium alignment for a velocity field, while diverging or converging flow, twisting flow, and recirculating flow would be the corresponding deformations of splay, twist, and bend, respectively.

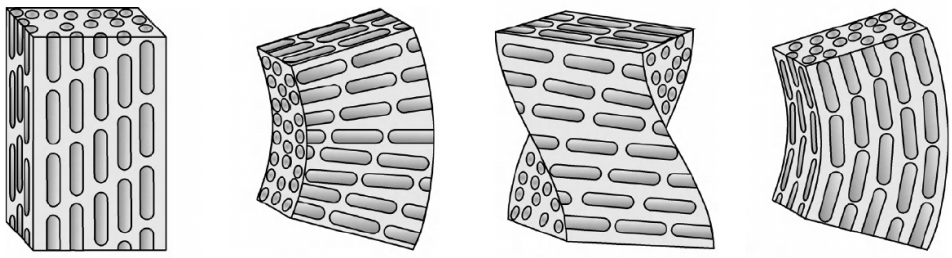

(a) Equilibrium (b) Splay, k_{11} (c) Twist, k_{22} (d) Bend, k_{33}

Figure 4.2: Liquid crystal alignment modes: equilibrium (a) and deformation modes splay, twist, and bend (b), (c), and (d). Obtained from [34].

4.2 Computation of Velocity Topology

Deformation modes are quantified in liquid crystal physics using the molecular alignment vector field $\boldsymbol{n}$, which represents the average orientation of liquid crystal molecules at every point in space, as shown in Figure 4.3. Since $\boldsymbol{n}$ only captures molecular orientation, it is a unit vector. Frank-Oseen Theory decomposes the Helmholtz free energy density of a uniaxial nematic liquid crystal into a summation of contributions from splay, twist, and bend [35], which are each calculated as a transformation of $\boldsymbol{n}$. This free energy density is computed as follows:

$$f_f = \frac{1}{2}k_{11}\left(\boldsymbol{\nabla}\cdot\boldsymbol{n}\right)^2 + \frac{1}{2}k_{22}\left(\boldsymbol{n}\cdot\boldsymbol{\nabla}\times\boldsymbol{n}\right)^2 + \frac{1}{2}k_{33}\left(\boldsymbol{n}\times\boldsymbol{\nabla}\times\boldsymbol{n}\right)^2 \tag{4.1}$$

Individually, the contributions from splay, twist, and bend deformations are calculated as follows:

$$\text{Splay} = \frac{1}{2}k_{11}\left(\boldsymbol{\nabla}\cdot\boldsymbol{n}\right)^2 \tag{4.2}$$

$$\text{Twist} = \frac{1}{2}k_{22}\left(\boldsymbol{n}\cdot\boldsymbol{\nabla}\times\boldsymbol{n}\right)^2 \tag{4.3}$$

$$\text{Bend} = \frac{1}{2}k_{33}\left(\boldsymbol{n}\times\boldsymbol{\nabla}\times\boldsymbol{n}\right)^2 \tag{4.4}$$

where k_{11}, k_{22}, k_{33} are the elastic moduli corresponding to the free energy contributions of splay, twist, and bend, respectively.

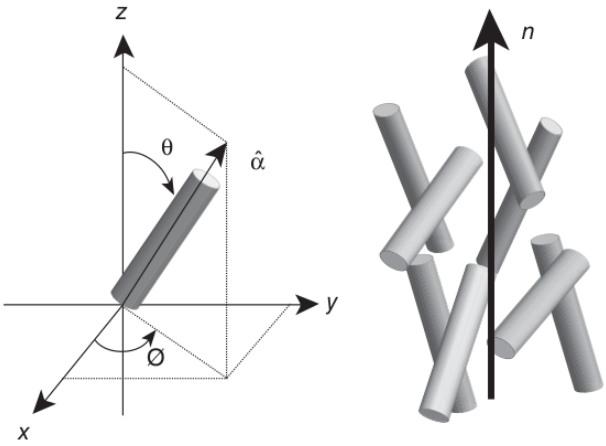

Figure 4.3: Left: orientation of a liquid crystal molecule. Right: molecular alignment vector $\boldsymbol{n}$ representing average orientation of a group of molecules. Obtained from [36].

To perform an analogous computation for fluid flow, it is first necessary to define an alignment vector $\boldsymbol{n}$ for the velocity of the flow. The modes of flow discussed in Section 4.1 are based on spatial variation in the direction of the velocity field, not variations in the magnitude of velocity. To isolate changes in the direction of the velocity field, the velocity vector can be decomposed into its magnitude (scalar quantity) and direction (vector quantity). The velocity direction can be isolated as follows:

$$\boldsymbol{n_v} = \frac{\boldsymbol{v}}{\sqrt{\boldsymbol{v} \cdot \boldsymbol{v}}} \tag{4.5}$$

which is denoted as $\boldsymbol{n_v}$ and will be referred to as the velocity alignment vector to emphasize its analogy with the molecular alignment vector $\boldsymbol{n}$. The velocity alignment vector can then be used in Equations 4.2 - 4.4 to compute splay, twist, and bend for the flow of a fluid. As a first approach to the analysis of the deformation modes for velocity alignment, it is arbitrarily chosen that the elastic moduli $k_{ii} = 2$ to equally weigh the values of splay, twist, and bend and eliminate the factor of $\frac{1}{2}$ for each deformation mode.

The velocity alignment vector can be used to quantitatively identify regions of distinct flow modes. It is hypothesized that high values of splay will correspond to expanding or contracting flow, high values of twist will correspond to twisting flow, and high values of bend will correspond to recirculating flow. Low values of each deformation mode should correspond to unidirectional flow.

4.3 Determining Compartments using Velocity Topology

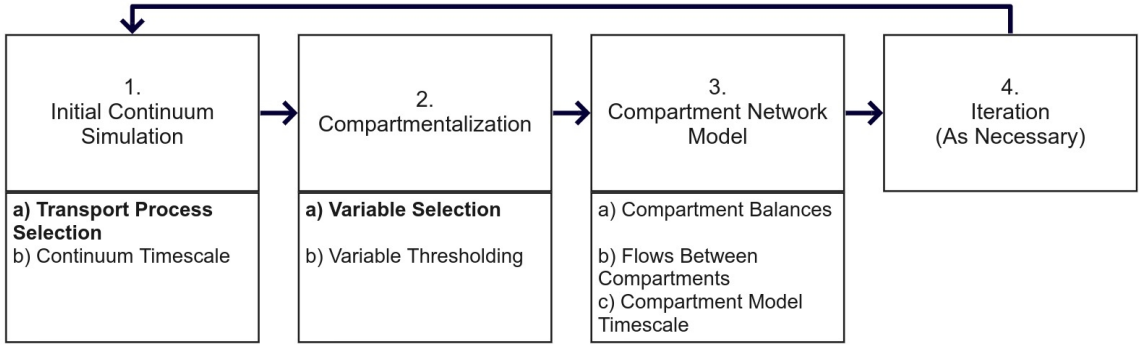

Figure 4.4: Flow chart highlighting areas where topological compartmentalization deviates from existing compartment modeling procedure.

Topological compartmentalization follows the overall process discussed in Section 2.3.2, with major changes highlighted in Figure 4.4 and discussed as follows:

1. **Initial Continuum Simulation**: To perform topological compartmentalization, it is necessary to obtain the steady-state or pseudo-steady-state velocity field of a continuous fluid phase. To do so, equations for the conservation of mass and momentum must be formulated and solved. These conservation equations must capture any transport phenomena with timescales on the order of the convective timescale.[2] Transport phenomena with longer timescales can be neglected in this simulation. These might include energy transport, transport of mass and momentum of a dispersed phase such as in an Euler-Euler or Euler-Lagrange model, diffusion of mass and momentum, and physical or chemical reactions.

2. **Compartmentalization**: The novelty of the topological compartmentalization approach presented in this work is the use of topological quantities as the variables for compartmentalization. These quantities must be computed from the continuum

[2]The reader is directed to ref. [37] for a comprehensive and systematic approach to scaling analysis, including unsteady problems.

simulation result using Equations 4.2 - 4.5 as discussed in Section 4.2. It is necessary to exclude regions of the domain where the velocity magnitude $\sqrt{\boldsymbol{v} \cdot \boldsymbol{v}}$ is zero and the velocity alignment vector is degenerate, such as at no-slip boundaries. This can be done by excluding regions where $\sqrt{\boldsymbol{v} \cdot \boldsymbol{v}}$ is approximately zero based on the numerical precision used to compute the continuum solution. Different approaches can be used to threshold topological quantities. In this work, thresholding is done manually, as discussed in Section 5.5.

3. **Compartment Network Model**: As an initial approach, the compartment network model is developed as discussed in Section 2.3.3. This work does not consider modelling of turbulent flows, so turbulent exchanges between compartments as discussed in Section 2.3.4 are neglected. However, works that build on this approach would be able to incorporate one of the existing methods for estimating turbulent flows. Compartment balances that treat each compartment as well-mixed, as in Equation 2.15, are initially used for the compartment network model. However, as will be discussed in Section 6.2, this approximation is not valid for compartments dominated by unidirectional flow. Section 6.3 proposes modelling unidirectional flow compartments as a series of CSTRs. Other simple reactor models are possible, which may be a focus for future work.

4. **Iteration**: As discussed in Section 2.3.2, a user may iterate through the process of continuum simulation, compartmentalization, and compartment network modelling. This iteration occurs when the phenomena captured in the compartment model are suspected to have significantly affected the velocity field. The focus of this work is on compartmentalization and compartment network development. Therefore, iteration is not considered in detail.

Chapter 5

Development of Topological Compartmentalization Algorithm

The goal of this chapter is to introduce a topology-based algorithm for compartmentalization. First, a test case is introduced and the distinct flow regions that the compartmentalization should capture are identified. Next, conventional fluid quantities that might be used for compartmentalization are considered and shown to fail to identify the distinct flow regions of interest. The fluid alignment vector introduced in Section 4.2 is computed, and this quantity is shown to capture the flow regions through its curl and then through splay and bend. The combined local alignment deformation measure is computed, and thresholding of this quantity is shown to generally distinguish recirculation, splay, and unidirectional flow.

5.1 Test Case: Cylindrical Vessel with Varying Cross-section

In order to develop a compartmentalization method based on flow alignment topology, a simple test case was chosen consisting of a cylindrical pipe inlet leading into a larger cylindrical vessel with an open outlet. A cross-section of the geometry in the XZ-plane is shown in Figure 5.1. The inlet pipe has an internal radius of 0.1 m and a length of 0.5 m, while the cylindrical vessel has a radius of 0.3 m and a length of 1.5 m. The test case has axial symmetry around the Z-axis, although the full 3-D geometry was simulated. For simplicity of analysis, cross-sections cutting through the center line are shown. Figure 5.1

displays the inlet boundary as the left-most vertical line (red), the outlet boundary as the right-most vertical line (blue), and the wall boundaries as the remaining edges (green).

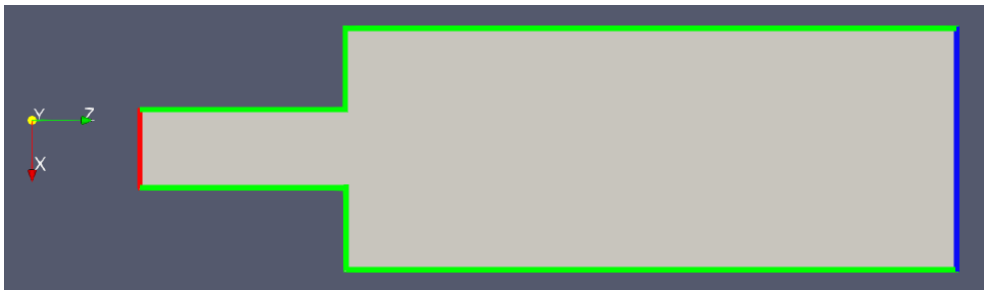

Figure 5.1: Geometry of test case used for investigation of topological compartmentalziation.

The case geometry was meshed using `Gmsh`. A 2-D mesh was created for a cross-section of the case in the XY-plane and is shown in the left of Figure 5.2. The innermost portion of the 2-D mesh is contained in a regular hexagon with vertices located 0.05 m from the center point, and tetrahedral elements were created for 10 evenly-spaced steps from the centre to the vertices. Lines from the centre point through the hexagon vertices were extended to the inner and outer cylinder circumferences. Mesh elements were created for 10 evenly-spaced steps from the hexagon edges to the inner cylinder circumference and 15 evenly-spaced steps from the inner cylinder circumference to the outer cylinder circumference. The 2-D mesh was then extruded in the Z-direction with 15 evenly-spaced elements for the smaller inlet region and 100 evenly-spaced elements for the larger vessel region, as shown the right of Figure 5.2. The mesh has a total number of elements of 204000.

The inlet boundary condition for velocity was a fixed value of $1\,\mathrm{m\,s^{-1}}$ in the z-direction. No-slip boundary conditions were used for the walls and an initial condition of zero velocity was set throughout the domain. For the outlet, a pressure condition was used, with the outlet pressure set to 0 Pa. The zero-gradient boundary condition for pressure was applied to the inlet and walls.

A kinematic viscosity of 0.01 Pa s was set for the fluid. Using the inlet velocity and larger vessel diameter, a maximum Reynolds number of 30 is expected, so the flow is assumed to be laminar.

The continuum solution for the test case was obtained through numerical solution using the `OpenFOAM` implementation of the SIMPLE method [38]. The SIMPLE method solves the Navier-Stokes equations numerically by discretizing and separating them into a momentum equation and a pressure equation. For both equations, convergence criteria for

residuals were set to 10^{-6} for absolute tolerance and 0.1 for relative tolerance. Timesteps of 0.01 s were taken and convergence was reached after 1.69 seconds of simulation time. The continuum solution is shown in Figure 5.3, which visualizes the velocity field through streamlines and velocity magnitude ($\sqrt{\boldsymbol{v} \cdot \boldsymbol{v}}$).

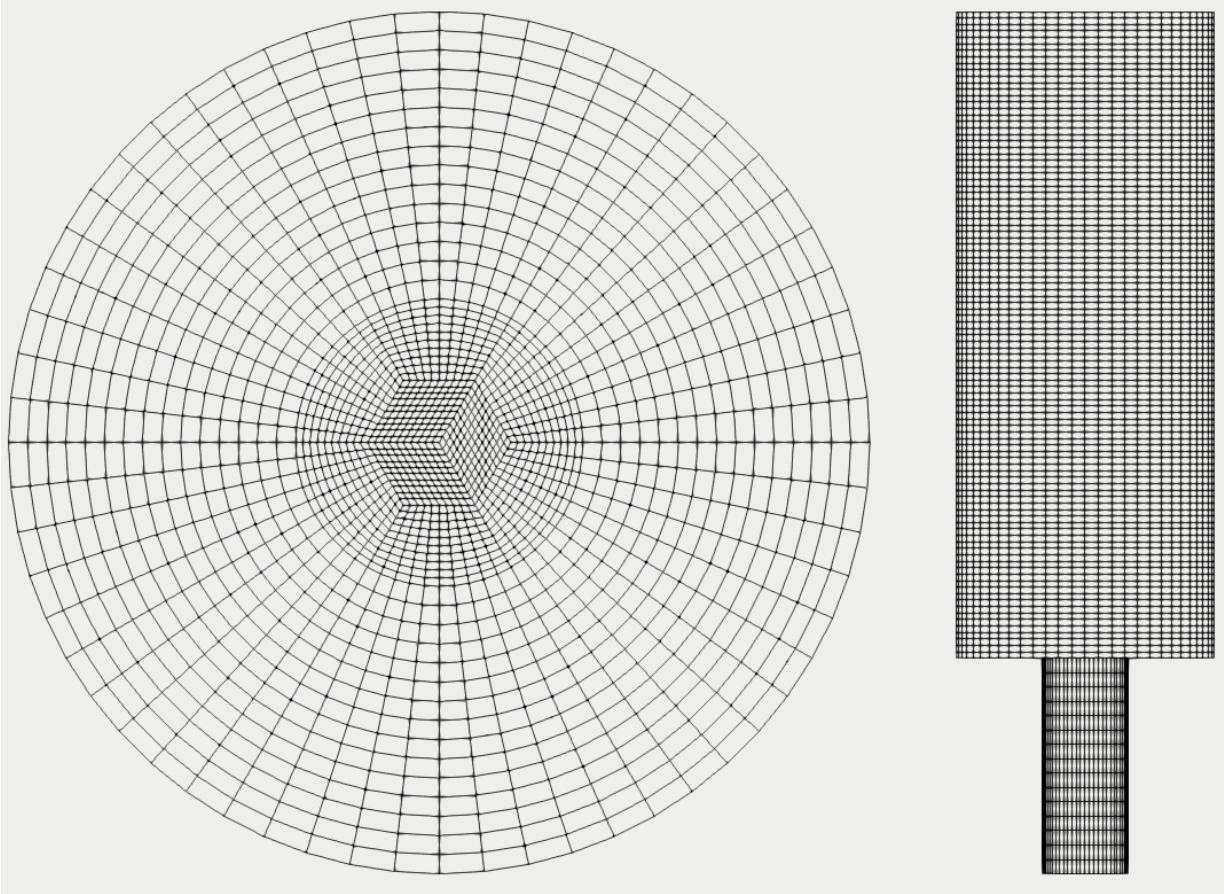

Figure 5.2: Mesh for case geometry visualized with cross-section in XY-plane (left) and through the centre of the case in the XZ-plane (right).

From the velocity visualization in Figure 5.3, the following distinct flow features are identified:

Inlet - Parabolic, Unidirectional Flow: flow through the inlet pipe develops into highly unidirectional flow in the Z-direction, varying from a velocity of 0 m/s at the walls to 2 m/s at the centre of the pipe.

Outlet - Parabolic, Unidirectional Flow: similar to the inlet, flow through the larger vessel develops to unidirectional flow in the Z-direction for the top half of the vessel.

Recirculation Zone - Recirculatory Flow: at the edge of the larger vessel near the inlet, recirculating flow is observed. This flow is much slower than the flow through the centre of the case. It should be noted that this is one single donut-shaped region around the Z-axis.

Expansion Zone - Diverging Flow: at the centre of the recirculation zone between the inlet and outlet, the fluid slows down due to the increase in cross-sectional area. This behaviour aligns with the splay deformation mode.

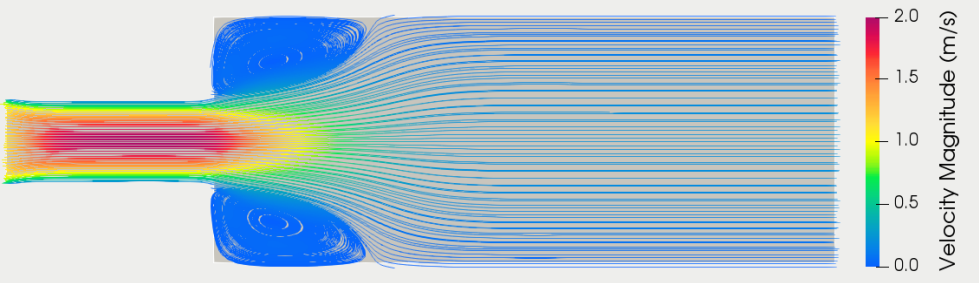

Figure 5.3: Visualization of velocity streamlines and velocity magnitude through the test case.

Based on this identification of the distinct flow features, the proposed goal of the topology-based compartmentalization is to capture these flow features in separate compartments.

5.2 Consideration of Fluid Quantities

As discussed in Section 3.1.2, velocity components are commonly used as quantities for compartmentalization. To demonstrate the need for the use of flow alignment topology for compartmentalization, compartmentalization based on the velocity field is first considered. In addition to the velocity field, presented in this section as velocity magnitude ($\sqrt{\boldsymbol{v} \cdot \boldsymbol{v}}$), vorticity ($\boldsymbol{\nabla} \times \boldsymbol{v}$) and velocity gradient ($\boldsymbol{\nabla v}$) are also considered as possible quantities for compartmentalization. Visualizations of these quantities using logarithmic scales were found to be most useful and thus this scale was used for the following visualizations.

5.2.1 Velocity Magnitude

Velocity magnitude is shown in Figure 5.4. Based on the data obtained from the continuum model and Figure 5.3, recirculation zones can be identified at the edge of the vessel near the inlet as having a velocity magnitude between 0.02 and 0.2 m/s. However, the use of velocity magnitude alone cannot distingish between these regions and the slower flow region near the walls of the outlet resulting from the no-slip condition. This suggests additional information is necessary for effective compartmentalization.

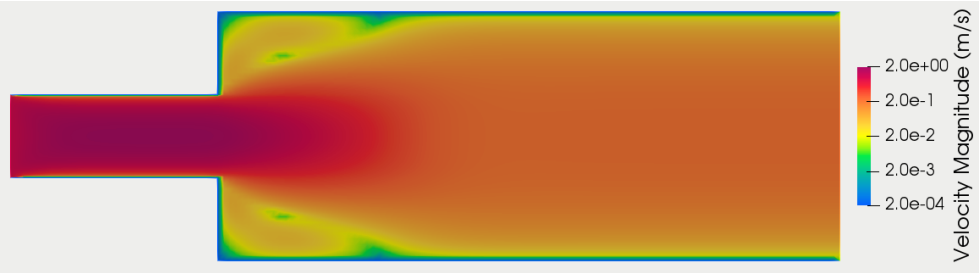

Figure 5.4: Visualization of velocity magnitude ($\sqrt{\boldsymbol{v} \cdot \boldsymbol{v}}$) through the test case.

5.2.2 Vorticity

Vorticity is mathematically defined as the curl of velocity ($\boldsymbol{\nabla} \times \boldsymbol{v}$). It is a local measure of the rate of rotation of a fluid element. Consequently, it was hypothesized to provide a useful quantity for compartmentalization, as it might be highest in recirculation regions and lowest in regions of unidirectional flow. However, this was not observed, as shown in Figure 5.5. Since vorticity is minimal along the centre of the case due to the axisymmetric geometry, no rotation should be observed at the center. However, vorticity is seen to be greatest between the centre and the walls of the inlet. This results from the shear stress near the walls of the inlet that produce a high velocity gradient perpendicular to the direction of flow. It does not seem feasible to identify the recirculation regions from the vorticity plot.

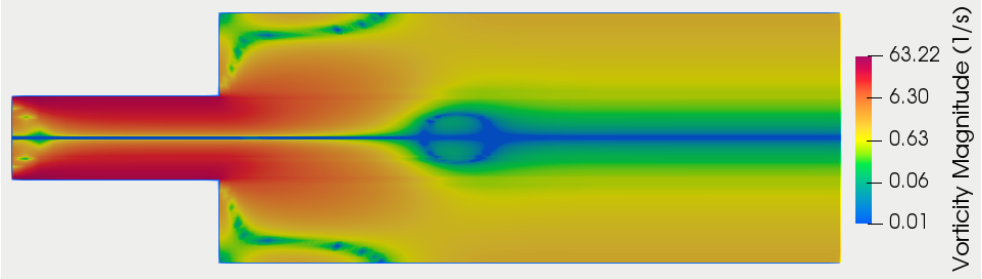

Figure 5.5: Visualization of the magnitude of vorticity ($\boldsymbol{\nabla} \times \boldsymbol{v}$) through the test case.

5.2.3 Velocity Gradient

For Newtonian fluids, the velocity gradient is equivalent to the strain rate tensor and is proportional to shear stress following Newton's law of viscosity. The magnitude of a tensor $\boldsymbol{\tau}$ is defined by [33]:

$$|\boldsymbol{\tau}| = \sqrt{\frac{1}{2}\boldsymbol{\tau} : \boldsymbol{\tau}^T} = \sqrt{\frac{1}{2}\sum_i \sum_j \tau_{ij}^2} \tag{5.1}$$

The plot of the magnitude of the velocity gradient, Figure 5.6, is qualitatively very similar to that of the magnitude of vorticity. Again, the highest values are observed near the walls of the inlet due to the higher shear stress, and regions of recirculation and unidirectional flow are not clear.

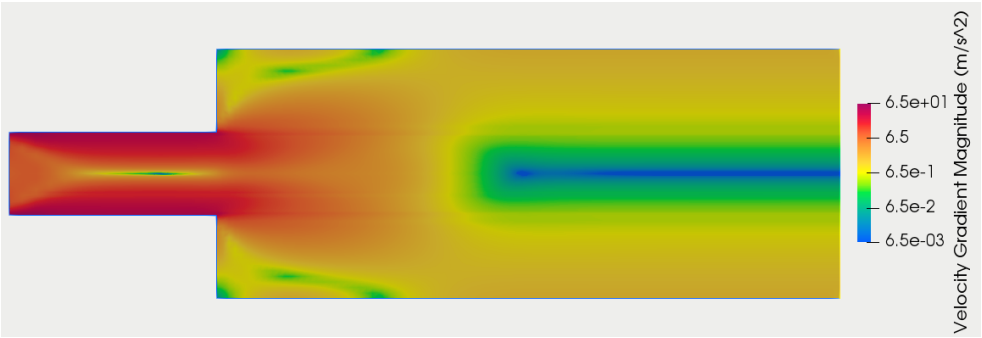

Figure 5.6: Visualization of the magnitude of the velocity gradient ($\boldsymbol{\nabla v}$) through the test case.

5.3 Analysis of Fluid Alignment Vector

As introduced in Equation 4.5, the fluid alignment vector field was calculated by normalizing the velocity vector at every point in space. Like velocity, it can be visualized using streamlines. However, since the fluid alignment vector has a magnitude of unity everywhere and has the same direction as velocity, the resulting visualization would be identical to Figure 5.3 without any variation in colouring for its magnitude.

As an alternative, the fluid alignment vector can also be considered by plotting the magnitude of its curl ($\boldsymbol{\nabla} \times \boldsymbol{n_v}$), as shown in Figure 5.7. The magnitude of the curl of a vector represents how much an object placed in the vector field would rotate, with the axis of rotation being the direction of the curl. Therefore, the magnitude of the curl of the fluid alignment vector represents the extent to which the fluid alignment vector changes direction, or how much the velocity of the fluid changes direction. This can be seen in Figure 5.7, where the highest values of the curl of the velocity alignment vector are observed in the recirculation regions identified in Figure 5.3, while the lowest values are observed in the unidirectional inlet and outlet regions. This suggests the use of the velocity alignment vector offers a promising approach for topological compartmentalization.

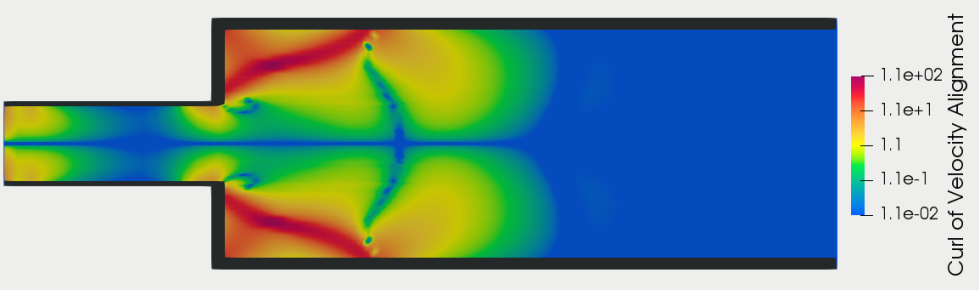

Figure 5.7: Visualization of the curl of the velocity alignment vector ($\boldsymbol{\nabla} \times \boldsymbol{n_v}$) through the test case.

The black areas of this plot indicate regions where the curl of the velocity alignment vector is undefined. This occurs when the velocity approaches zero and the direction of velocity becomes degenerate. These regions are observed near the walls due to the no-slip condition, which would occur in many fluid flow problems. The threshold below which velocity is considered zero and the velocity alignment vector is undefined is proportional to the numerical tolerance of the solver used in the continuum simulation. Regions where velocity is near zero can be neglected from the compartment model since they will not mix significantly with the bulk flow.

5.4 Analysis of Vector Topology Quantities

Recalling that the fluid alignment vector $\boldsymbol{n_v}$ is used in place of $\boldsymbol{n}$ in Equations 4.2 - 4.5, these equations were used to calculate splay, twist, and bend for the test case. It was hypothesized that these quantities should correspond to distinct flow features that could therefore be used for topological compartmentalization.

Splay is plotted in Figure 5.8 and is expected to occur where the cross-sectional area for flow expands or shrinks, such as where a pipe changes diameter. In the test case, this flow behaviour is observed at the center of the domain where flow from the inlet enters and spreads outwards. As observed in the figure, a large area of splay is observed in this center region as expected. Interestingly, the highest values of splay are observed in the recirculation region.

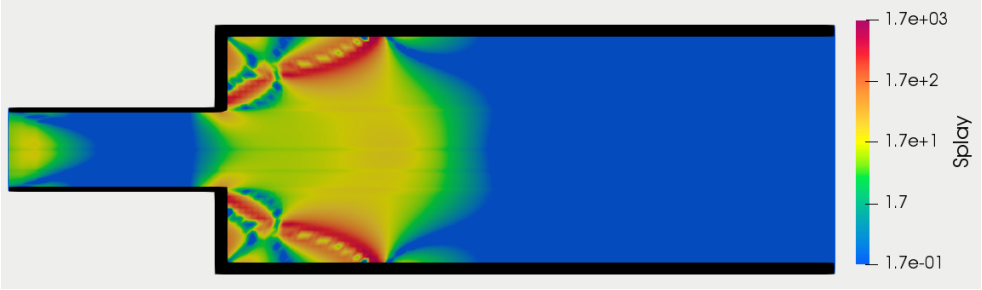

Figure 5.8: Visualization of splay $(\boldsymbol{\nabla} \cdot \boldsymbol{n_v})^2$ through the test case.

Bend is plotted in Figure 5.9 and is expected to correspond to areas where flow turns, such as in a recirculation region. As expected, high values of bend are observed to be isolated to the recirculation regions previously identified. However, high values of bend do not capture the entire recirculation region, particularly close to the walls. Despite this, bend provides a good initial estimate for the location of the recirculation region.

Reviewing Equation 4.3 for twist, twist is negligible when the term within the brackets $(\boldsymbol{n_v} \cdot \boldsymbol{\nabla} \times \boldsymbol{n_v})$ is small. This is the dot product of $\boldsymbol{n_v}$ and the curl of $\boldsymbol{n_v}$; that means that it measures the rotation of $\boldsymbol{n_v}$ about an axis equal to the direction of $\boldsymbol{n_v}$. Since the test case is axisymmetric about the Z-axis and the predominant flow direction is in Z, twist was not expected to be a significant feature within the test case. As expected, the highest value of twist observed (10^{-1}) was much less than the values of 10^3 and 10^4 observed for splay and bend, respectively. Consequently, a visualization of twist is not included.

Overall, the visualization of the magnitudes of splay and bend are observed to capture the distinct flow features of interests. High values of bend correspond to regions where the

flow recirculates. Low values of bend with moderate values of splay correspond to regions where flow expands. Low values of both quantities correspond to regions of unidirectional flow. Based on these observations, it was concluded that these deformational measures can be used for topological compartmentalization. From here forward, their summation is referred to as the *local alignment deformation measure*.

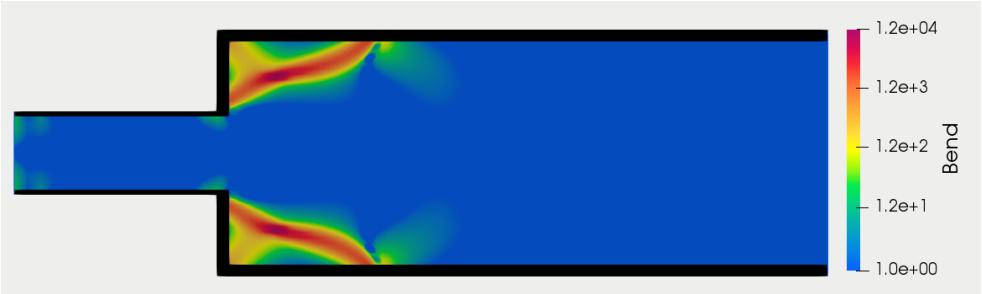

Figure 5.9: Visualization of bend $(\boldsymbol{n} \times \boldsymbol{\nabla} \times \boldsymbol{n})^2$ through the test case.

5.5 Analysis of Local Alignment Deformation

The local alignment deformation measure, corresponding to the quantity f_f from Equation 4.1, is the sum of splay, twist, and bend of the velocity alignment vector field. This quantity was computed for the test case and is shown in Figure 5.10. This quantity is generally able to distinguish the recirculation regions with $f_f > 100$, diverging flow region with $1 < f_f < 100$, and unidirectional flow regions with $f_f < 1$.

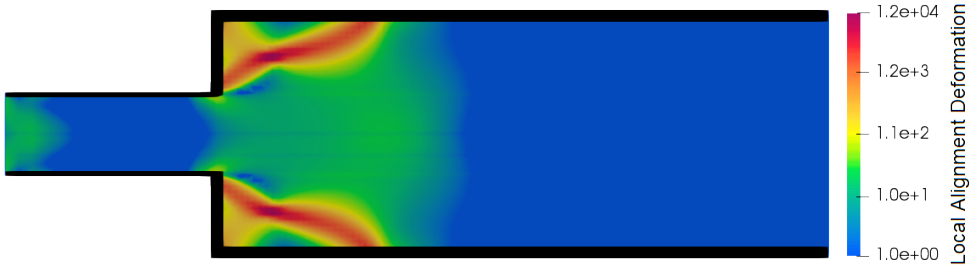

Figure 5.10: Visualization of local alignment deformation through the test case.

Local alignment deformation was identified as the quantity to be used for compartmentalization based on a qualitative assessment of how well the measure identified the distinct

flow regions identified in Figure 5.3. This quantity will be used in the following chapter as the quantity for compartmentalization. Splay, twist, bend, and local alignment deformation as introduced in this work are novel quantities both for the topological analysis of fluid flow and for compartmentalization.

Chapter 6

Application and Validation of Topological Compartmentalization Algorithm

The goals of this chapter are to use the topologically-informed compartmentalization approach developed in Chapter 5 to construct a compartment model and to validate the compartmentalization approach and compartment model against a continuum simulation. First, the process of the compartmentalization approach is summarized. Compartments are identified by applying this approach to the test case introduced in Section 5.1. These compartments are discussed in relation to the flow modes previously identified. Next, the RTDs predicted by the continuum simulation and compartment model are computed and compared. The RTD of the compartment model is observed to have a lower mean residence time and greater variance and skewness, which is attributed to approximating unidirectional compartments as well-mixed. Following this discussion, the compartment model is modified to approximate each of the unidirectional compartments as a series of CSTRs. As expected, increasing the number of CSTRs-in-series biases the compartment model towards PFR-like behaviour, reducing the RTD variance and skewness; however, the mean residence time remains unchanged, so significant deviation from the continuum simulation RTD still exists. The effect of varying the values chosen for thresholding local alignment deformation f_f is considered; changing the lower threshold of f_f from 1 to 10 is observed to have an insignificant effect on the compartment model RTD. Finally, RTD computation times for the continuum simulation and compartment models are compared to quantify the reduction in computation costs for the compartment model: RTDs for the compartment model were computed 400-900 times faster than the RTD for the continuum

simulation.

6.1 Initial Compartmentalization

The initial compartmentalization (referred to as compartmentalization 1) of the test case was carried out by thresholding the local alignment deformation based on the qualitative analysis discussed in the previous chapter. The algorithm for topology-based compartmentalization can be summarized as follows:

Computation of Local Alignment Deformation: As introduced in Section 4.2, computation of local alignment deformation requires the computation of the velocity alignment vector $\boldsymbol{n_v}$, following Equation 4.5. This eliminates areas where velocity magnitude is approximately zero, since the direction of velocity is degenerate for these areas. Next, splay, twist, and bend are computed from Equations 4.2 - 4.4 by substituting $\boldsymbol{n_v}$ for $\boldsymbol{n}$. Finally, the local alignment deformation measure is computed as the sum of splay, twist, and bend of the flow alignment vector field.

Thresholding of Alignment Deformation: As discussed in Section 5.5, local alignment deformation was thresholded to separate the recirculation region ($f_f > 100$), splay region ($1 < f_f < 100$), and unidirectional flow regions ($f_f < 1$). In this work, the thresholding is done manually; however, this can be automated based on standard image processing techniques [39]. One possible approach is Otsu's method, which can identify multiple threshold levels to segment an image based on a histogram of the image's intensity. The result of thresholding the test case is shown in Figure 6.1.

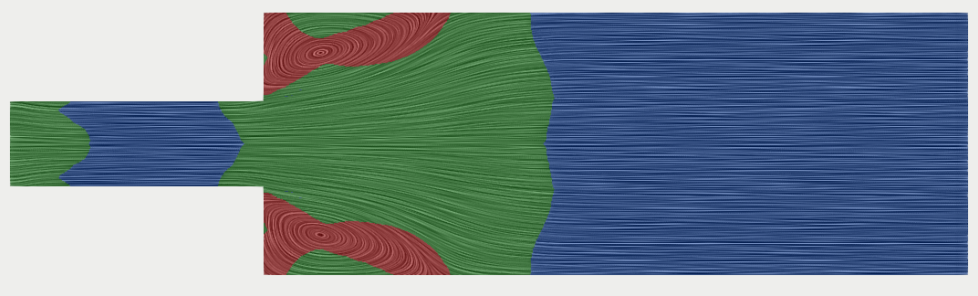

Figure 6.1: Thresholding of local alignment deformation over velocity streamlines: Red for $f_f > 100$, green for $1 < f_f < 100$, and blue for $f_f < 1$.

Compartment Segmentation: A condition for compartment models to be physically valid is that compartments are contiguous, meaning each compartment is enclosed by a single continuous surface. Thresholded sections of the domain may include noncontiguous regions. In this case, examples of noncontiguous regions are the inlet and outlet regions, which are both unidirectional flow regions but are separated by the splay region. Therefore, the noncontiguous regions that can be identified in Figure 6.1 must be segmented into compartments as shown in Figure 6.2.

Compartment Classification: After the compartments have been segmented, they can be classified based on the flow mode that is most dominant within the compartment. Flow modes include unidirectional, diverging or converging, recirculating, twisting, and stagnant, as discussed in Section 4.1.

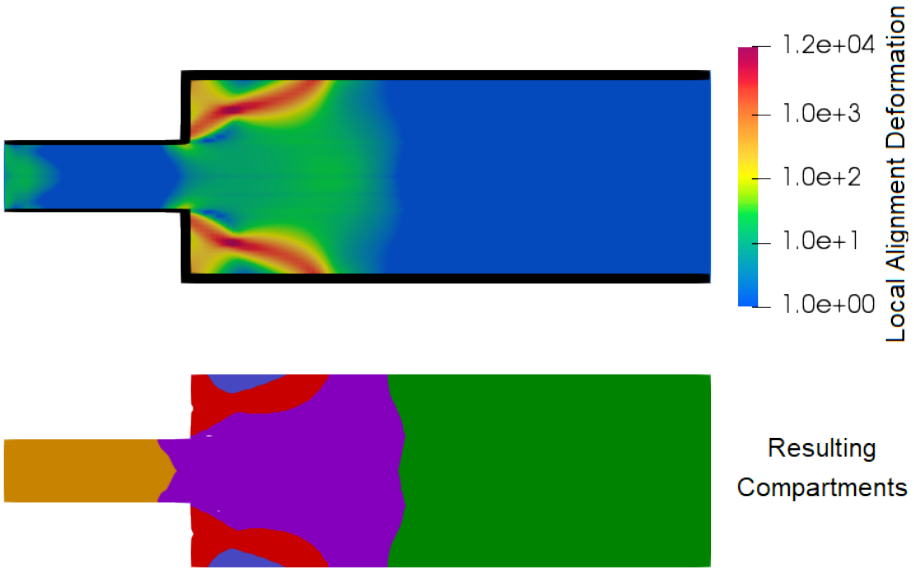

Figure 6.2: Visualization of compartments resulting from compartmentalization 1. Plot of local alignment deformation over the test case (top) and resulting compartments used for the initial compartment model (bottom). The compartments are identified as follows: orange - inlet, green - outlet, purple - splay, red - recirculation, blue - stagnation zone.

The resulting compartments from the test case are shown in Figure 6.2 with compartment classifications identified based on the discussion in Section 5.4:

Unidirectional Compartments: Flow can be classified as unidirectional based on having low values of local alignment deformation, which is the sum of splay, twist, and bend. The unidirectional regions in the test case are flow through the inlet and flow to the outlet, which are shown as the orange and green regions in Figure 6.2. These correspond to the inlet and outlet zones identified in Section 5.1.

Diverging Compartment: Flow can be classified as converging or diverging based on having moderate or high values of splay and low values of bend. The distinction between converging and diverging flow is whether the cross-sectional area of the compartment decreases or increases in the direction of flow. The diverging region in the test case occurs where flow from the inlet reaches the vessel and spreads outwards to occupy the increase in cross-sectional area, which is shown as the purple region in Figure 6.2. This corresponds to the expansion zone identified in Section 5.1.

Recirculating Compartment: Flow can be classified as recirculating based on having high values of bend, which correspond to a high value of local alignment deformation in this case. The recirculating region occurs around the diverging region where a vortex is generated, which is shown as the red region in Figure 6.2. This mostly corresponds to the recirculation zone identified in Section 5.1.

Stagnation Compartment: Flow can be classified as stagnant based on a low value of velocity magnitude. Near the wall of the vessel, backflow from the recirculating zone has a relatively constant velocity direction. As a result, it has a lower value of bend and is not classified as recirculating. This is shown in the blue region in Figure 6.2.

6.2 Residence Time Distribution Comparison

To validate the compartmentalization completed in Section 6.1, the RTD from the resulting compartment model is compared to the RTD from the continuum solution presented in Section 5.1. The compartment model approximates the hydrodynamics of a system by modelling it as a network of ideally-mixed sub-domains. Therefore, the closer the RTD of the compartment model is to the RTD from a continuum solution, the greater the accuracy of the compartment model.

6.2.1 Residence Time Distribution Computation for Continuum Simulation

As discussed in Section 2.2, the RTD of a system can be obtained by simulating the transport of a passive scalar field T over a steady-state velocity field $\boldsymbol{v}$. Therefore, the RTD of the continuum solution was obtained by simulating the transport of a passive scalar using the `OpenFOAM` implementation of the scalar transport method [38]. This implementation solves Equation 2.9 over a fixed velocity field $\boldsymbol{v}$ input by the user. D_T is set to 0 so that the passive scalar T is transported by convection only. The initial condition $T = 0$ was set throughout the domain and the boundary condition $T = 1$ was set across the inlet. This simulation is analogous to a step input tracer experiment, as discussed in Section 2.2.

The goal of this simulation is to obtain a time profile of the average value of T at the outlet. This average value T_{out} is calculated as follows:

$$T_{out} = \frac{1}{A_{out}} \iint T dA \tag{6.1}$$

where A_{out} is the cross-sectional area of the outlet. After completing the simulation, the integration in Equation 6.1 was performed numerically in `ParaView` [40] following the tutorial for computing RTD in [41]. The resulting plot of T_{out} is shown in Figure 6.3. As time increases, the passive scalar value approaches a constant value of 1, indicating that the passive scalar has been transported throughout the test case.

Since this profile is from a step input, the RTD for the continuum solution is obtained by taking the derivative of T_{out} following Equation 2.8:

$$E(t) = \frac{dT_{out}}{dt} \tag{6.2}$$

This derivative was taken numerically using a simple first-order finite difference. The resulting continuum RTD is plotted in Figure 6.4.

6.2.2 Residence Time Distribution Computation for Compartment Model

The RTD of the compartment model was also obtained by simulating the transport of a passive scalar. To transport a passive scalar through the compartment model, the

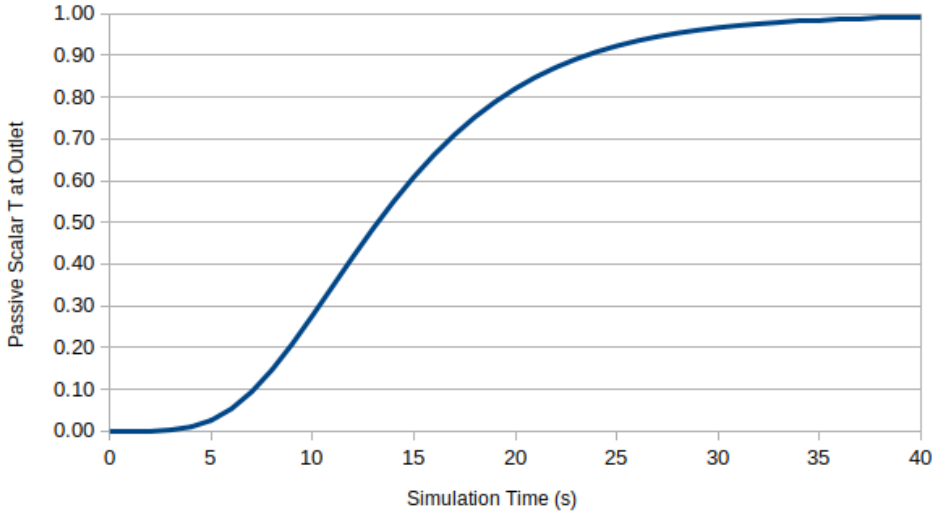

Figure 6.3: Time profile of passive scalar T across the outlet from simulated tracer experiment for continuum solution.

convection-diffusion equation (Equation 2.9) was combined with the general compartment mass balance shown in Equation 2.15:

$$V_i \frac{dT_i}{dt} = \sum_{j=1}^{n_c} (Q_{j\to i} T_j - Q_{i\to j} T_i) + Q_{in\to i} T_{in} - Q_{i\to out} T_i \tag{6.3}$$

where, in addition to the terms defined in Equation 2.15, T_i is the passive scalar value in compartment i, $Q_{in\to i}$ is the volumetric flow rate of material from the inlet to compartment i, $Q_{i\to out}$ is the volumetric flow rate of material from compartment i through the outlet, and T_{in} is the passive scalar value entering through the inlet. These terms are 0 if the compartment does not connect with the inlet or outlet. $c_{k,i}$ is replaced with T_i since only transport of the passive scalar is simulated.

Note that Q in this equation is the volumetric flow rate from convective fluxes since the test case was laminar, and that the reaction term in Equation 2.15 is 0 since the passive scalar does not react. This formulation treats each compartment as well-mixed. After compartments were identified as discussed in Section 6.1, volumes of each compartment V_i were calculated using the `Integrate Variables` filter in `ParaView` [40]. Volumetric flows between compartments $Q_{i\to j}$, from the inlet $Q_{in\to i}$, and to the outlet $Q_{i\to out}$ were computed

by integrating the flow velocity over the compartment boundaries following Equation 2.17. T_{in} was set to 1 and the initial condition $T_i = 0$ was set for each compartment.

Equation 6.3 for each compartment generates an initial value problem for a system of ODEs. This system was solved numerically using the `SciPy` implementation of the LSODA ODE solver [42]. Since the passive scalar was observed to reach a constant value after 40 seconds in Figure 6.3, the system of differential equations was solved over 40 seconds to obtain concentrations for each compartment over time. Again, since the concentration profiles are obtained from a step input, the RTD for the compartment model is obtained by taking the derivative of T in the outlet compartment as in Equation 6.2. The resulting compartment model RTD is plotted in Figure 6.4.

6.2.3 Residence Time Distribution Comparison

As references for RTD analysis, the residence time distributions for a single ideal CSTR and single ideal PFR, each with the same volume and volumetric flow rate as the test case, were computed using Equations 2.13 and 2.14, respectively. These RTDs are compared with the RTDs for the compartment model and continuum solution in Figure 6.4.

The RTD of the continuum simulation has a mean residence time t_m of 14.1 s and has a slight right skew ($s^3 = 16.0\ \text{s}^3$), resulting in the mode residence time of 10.5 s. The compartment model has a lower mean residence time ($t_m = 10.6$ s), a larger variance ($\sigma^2 = 61.3\ \text{s}^2$ vs $40.7\ \text{s}^2$), and a much greater skewness ($s^3 = 28.6\ \text{s}^3$ vs $s^3 = 16.6\ \text{s}^3$), which shifts the mode residence time to the left to 4.3 s. A full comparison of the mean, variance, and skewness of the RTDs is presented in Table 6.1. The deviation from the lower mean residence time and greater skewness is quite clear in Figure 6.4, which shows that the compartment model predicts a bias towards well-mixed behavior relative to the more accurate continuum model. This suggests that either the compartmentalization scheme or the well-mixed assumption for modelling the compartments is not optimal.

Table 6.1: Comparison of moments of RTDs for continuum solution and compartment model.

RTD Source	Mean t_m (s)	Variance σ^2 (s^2)	Skewness s^3 (s^3)
Continuum Solution	14.1	40.7	16.6
Compartment Model	10.6	61.3	28.6

As stated in Section 6.2, the compartment model is formulated based on both the compartmentalization method and the volume-averaged model for each compartment and the

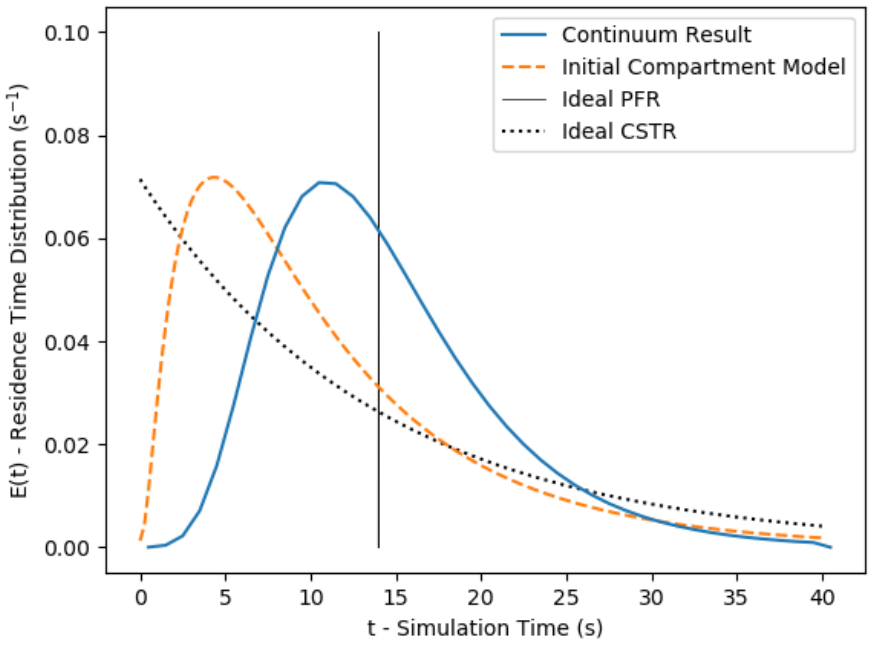

Figure 6.4: Comparison of RTDs for continuum solution and compartment model with RTDs for idealized PFR and CSTR as reference.

flows between them. Traditionally, the volume-averaged model is based on the assumption that each compartment is ideally-mixed, similar to an ideal CSTR. From re-examination of the compartmentalization in Figure 6.2 and the continuum result in Figure 5.3, two compartments with primarily unidirectional flow exist: the inlet and outlet compartments. Unidirectional flow is poorly approximated by an ideal-mixing assumption; instead, any material that enters a unidirectional flow requires time to be convected to the outlet before it can exit. The result of having these two compartments treated as well-mixed is that the resulting RTD is shifted toward the distribution of a CSTR, i.e. with a lower mode residence time and greater variance and right skew.

Since the proposed compartmentalization approach is based on the topology of the flow, it is feasible to use this topological information to distinguish between unidirectional regions and recirculatory regions based on the local alignment deformation. Subsequently, a nontraditional compartmental model may be intuitively developed taking account the differences in flow within each compartment. Furthermore, these different regions should

have different mixing behaviours: while recirculatory regions are likely well-mixed, unidirectional regions behave more like PFRs. Therefore, it would be justified to model unidirectional compartments as PFRs rather than as CSTRs.

PFR models are typically not zero-dimensional like that of ideal CSTRs, and instead include a one-dimensional spatial variation. Thus it is not optimal to treat unidirectional compartments as ideal PFRs, as this would result in solving a system of PDEs instead of ODEs, which eliminates the major justification for using a compartment model. Instead, since an ideal PFR can be approximated as a series of CSTRs, unidirectional compartments could likewise be modelled as a series of CSTRs instead of a single CSTR.

6.3 Modelling Unidirectional Compartments as a Series of CSTRs

As discussed in Section 6.2, the RTD of the compartment model might be improved by modelling the unidirectional flow compartments as a series of CSTRs. This section will observe the effect of changing the number of CSTRs used to model these compartments on the resulting RTD for the compartment model. The other compartments with splaying and recirculatory flow are modelled as single CSTRs.

The compartmentalization used is same as shown in Figure 6.2. Due to their low local alignment deformation values ($f_f < 1$), the inlet and outlet compartments are identified as unidirectional flow compartments, as discussed in Sections 5.5 and 6.1. Therefore, these compartments are chosen to be modelled as a series of CSTRs. To model these compartments as a series of CSTRs, a mass balance was derived for each CSTR in the series. Within the CSTR series, the first CSTR receives all flows into the compartment and the last CSTR discharges all flows to neighboring compartments. The intermediary CSTRs each receive all the flow out of the previous CSTR and send all of their flow to the following CSTR. The final CSTR sends outflows to all neighboring compartments. This produces the following general series of mass balances for a CSTR-in-series compartment:

$$\frac{V_i}{n_{CSTR}}\frac{dT_{i,1}}{dt} = \sum_{j=1}^{n_c}\left(Q_{j\to i}T_j\right) + Q_{in\to i}T_{in} - Q_{i,total}T_{i,1} \tag{6.4}$$

$$\frac{V_i}{n_{CSTR}}\frac{dT_{i,\alpha}}{dt} = Q_{i,total}\left(T_{i,\alpha-1} - T_{i,\alpha}\right) \qquad \text{for} \quad 1 < \alpha < n_{CSTR} \tag{6.5}$$

$$\frac{V_i}{n_{CSTR}}\frac{dT_{i,n_{CSTR}}}{dt} = Q_{i,total}T_{i,n_{CSTR}-1} - T_{i,n_{CSTR}}\left(\sum_{j=1}^{n_c}\left(\ Q_{i\to j}\right) + Q_{i\to out}\right) \tag{6.6}$$

where, in addition to terms defined in Equations 2.15 and 6.3, n_{CSTR} is the number of CSTRs-in-series for each unidirectional flow compartment, $T_{i,\alpha}$ is value of the passive scalar in the αth CSTR-in-series of the ith compartment, and $Q_{i,total}$ is the total volumetric flowrate through the ith compartment.

The result of modelling unidirectional flow compartments as a series of CSTRs is shown in Figure 6.5 and the moments of the RTDs are listed in Table 6.2. As n_{CSTR} increases from 1 to 3, the variance of the compartment model RTD decreases from $61.3\,\mathrm{s}^2$ to $39.8\,\mathrm{s}^2$, which is approximately the variance of the continuum RTD ($40.7\ \mathrm{s}^2$), and the skewness decreases from $28.6\ \mathrm{s}^3$ to $24.3\ \mathrm{s}^3$, which is closer to the skewness of the continuum RTD ($16.6\,\mathrm{s}^3$). The mode residence time is observed to increase from $4.3\,\mathrm{s}$ to $7.5\,\mathrm{s}$. However, the mean residence time t_m is essentially unchanged, so a large deviation from the continuum model remains ($t_m = 10.9\ \mathrm{s}$ vs $t_m = 14.1\ \mathrm{s}$). Increasing n_{CSTR} further to 4 begins to give worse results, with an unchanged mean residence time, lower variance, and higher skewness. From Figure 6.5, increasing n_{CSTR} appears to generate a more narrow distribution, and the RTD begins to resemble a PFR-like spike. This makes sense given that as n_{CSTR} increases, the unidirectional flow compartments are being approximated as more like PFRs.

From this result, it is clear that the hydrodynamic approximation used for the compartments contributes to the overall error of the compartment model. This contribution is distinct from the contribution of error due to the compartmentalization method used to identify compartments. In this case, whether the unidirectional flow compartments are modelled as single CSTRs or CSTRs-in-series, neither approximation effectively captures the distribution of residence times resulting from the parabolic flow profiles in either compartment.

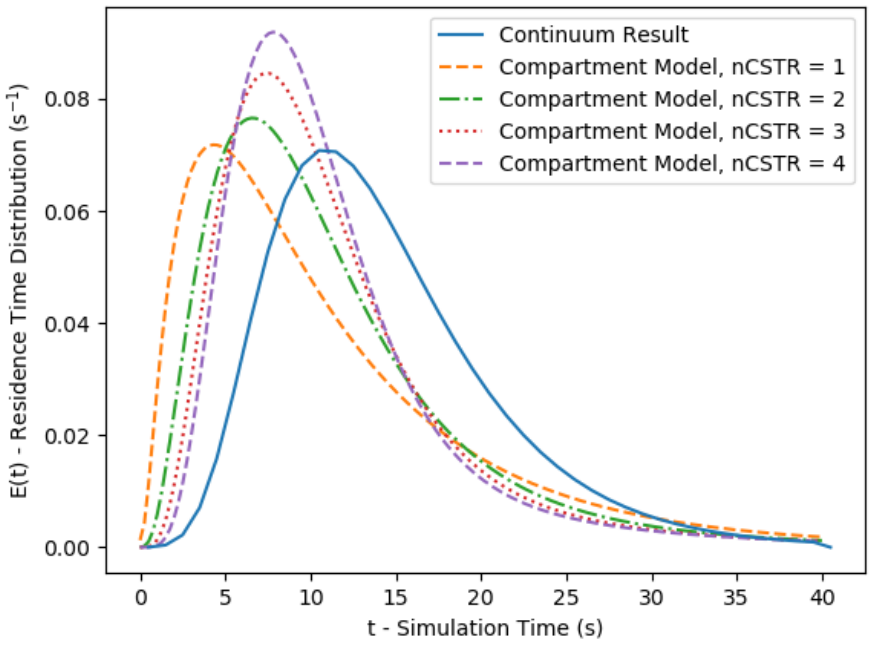

Figure 6.5: Comparison of residence time distributions (RTDs) for continuum solution and compartment model. The number of CSTRs-in-series used to model flow through the inlet and outlet compartments is varied from 1 to 4.

Table 6.2: Comparison of RTD moments for continuum solution and compartment model with unidirectional compartments approximated as a series of CSTRs.

RTD Source	n_{CSTR}	Mean t_m (s)	Variance σ^2 (s^2)	Skewness s^3 (s^3)
Continuum Solution	N/A	14.1	40.7	16.6
Compartment Model	1	10.6	61.3	28.6
Compartment Model	2	10.8	46.4	24.7
Compartment Model	3	10.9	39.8	24.3
Compartment Model	4	10.9	36.3	24.8

6.4 Variation of Compartmentalization Thresholding

The RTD of the compartment model will also be affected by the thresholding values chosen during compartmentalization. As identified in Section 5.5, local alignment deformation f_f

was thresholded arbitrarily at the values of 1 and 100 to capture the unidirectional, splay, and recirculation regions. These values can be adjusted to observe how significantly their selection affects the resulting RTD.

Since the splay region in Figure 6.2 is very large, the compartment model might be improved by decreasing its size. Therefore, the lower threshold value of local alignment deformation was increased from 1 to 10 in order to reduce the size of the splay compartment and increase the size of the unidirectional inlet and outlet compartments. The compartmentalization resulting from this change in thresholding, referred to as compartmentalization 2, is shown in Figure 6.6. This compartmentalization generated very small contiguous zones at the system boundaries near the inlet, recirculation, and dead zone compartments. These small zones were excluded from the compartment model for simplicity. Additionally, the grey region within the splay compartment had a low value of local alignment deformation ($f_f < 10$). To maintain the same network of compartments, the volume of this region was added to the splay compartment instead of modelling it as a separate compartment.

The RTD for the compartment model generated from compartmentalization 2 was computed and compared to the RTD of the compartment model resulting from the previous threshold values (i.e. compartmentalization 1). To simplify the comparison, inlet and outlet compartments for each model were each treated as two CSTRs-in-series, while the other compartments were treated as single CSTRs. The resulting RTDs are compared along with the RTD from the continuum solution in Figure 6.7.

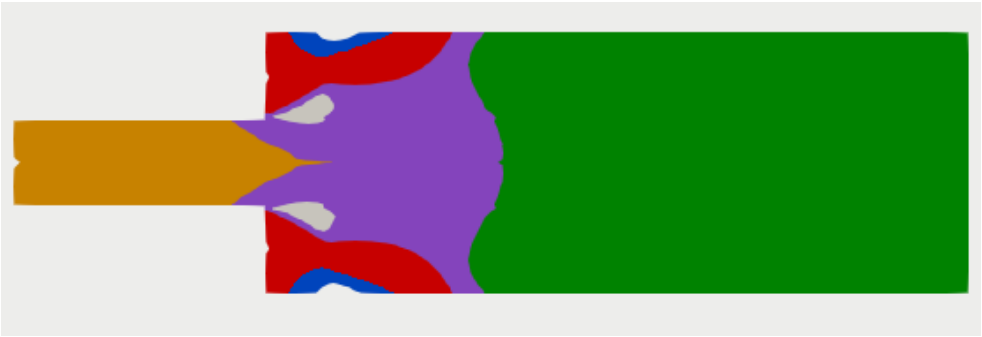

Figure 6.6: Visualization of compartments resulting from compartmentalization 2.

Very little difference is observed between the RTD of the compartment models, despite the change in thresholding values. This suggests that the volumes attributed to each compartment due to thresholding have a fairly minor impact on the resulting RTD as long

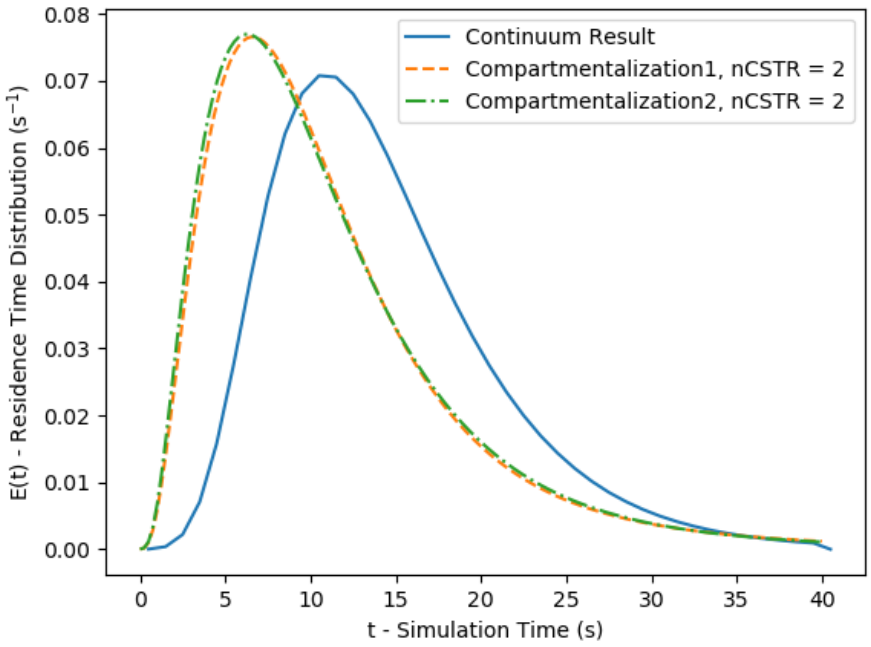

Figure 6.7: Comparison of RTDs for continuum solution and compartment models generated with developed with different compartmentalization thresholds.

as the underlying network of compartments is unchanged. The adjustment of the thresholding values does not help in resolving the remaining deviation between the continuum simulation RTD and the compartment model RTD.

6.5 Computation Time Comparison

A major benefit of compartment modelling is the potential reduction in computation time relative to continuum simulation. This benefit was quantified in this work by comparing RTD computation time for the compartment models and reference continuum solution presented in Sections 6.3 - 6.4. Compartmentalization 1 refers to the compartmentalization used in Section 6.3 (initial thresholding of local alignment deformation) and compartmentalization 2 refers to the compartmentalization used in Section 6.4 (modified thresholding of local alignment deformation). RTD computation times are compared in Table 6.3. RTD

computation for the compartment models was observed to be 400-900 times faster than RTD computation for the continuum model. This large speedup is consistent with literature: for example, ref. [16] report calculations for their compartment model were more than 4500 times faster than their reference continuum simulation.

Table 6.3: Comparison of computation times for obtaining RTDs for continuum solution and compartment models.

RTD Source	Compartmentalization	n_{CSTR}	RTD Computation Time (s)	Relative Speedup
Continuum Solution	N/A	N/A	63.39	N/A
Compartment Model	1	1	0.069	919
Compartment Model	1	2	0.120	528
Compartment Model	1	3	0.086	737
Compartment Model	1	4	0.154	412
Compartment Model	2	2	0.106	598

Chapter 7

Conclusions and Future Work

7.1 Conclusions

In this work, a topologically-informed compartmentalization approach is developed for the compartment modelling of multiphysics flows. The compartmentalization approach is applied to a test case, and the RTD of the resulting compartment model is compared to the RTD from a continuum simulation to validate the compartmentalization approach.

A velocity alignment vector was defined to quantitatively identify distinct flow modes. The computation of deformation modes splay, twist, and bend was observed to be effective for distiguishing between unidirectional, diverging/converging, and recirculating flow in a test case. Local alignment deformation f_f was defined as the sum of splay, twist, and bend of the velocity alignment field. f_f was thresholded at levels $f_f > 100$, $1 < f_f < 100$, and $f_f < 1$ to segment the test case domain into compartments of recirculating flow, diverging flow, and unidirectional flow. Splay, twist, bend, and local alignment deformation as introduced in this work are novel quantities both for the topological analysis of fluid flow and for compartmentalization.

The compartments produced by the thresolding of local alignment deformation were classified as unidirectional, diverging, recirculating, and stagnant. These compartments were used in a compartment model for the test case. The RTD of the compartment model and a reference continuum simulation were computed by simulating the transport of a passive scalar through the domain, which is analogous to a tracer experiment. The RTDs were compared quantitatively based on their first three moments. The RTD of the compartment model was found to have a lower mean residence time ($t_m = 10.6$ s vs

$t_m = 14.1\,\mathrm{s}$), a greater variance ($\sigma^2 = 61.3\,\mathrm{s}^2$ vs $40.7\,\mathrm{s}^2$) and a greater skewness ($s^3 = 28.6\,\mathrm{s}^3$ vs $s^3 = 16.0\,\mathrm{s}^3$) relative to the continuum solution. This deviation was attributed to the well-mixed approximation used for unidirectional flow compartments.

The modelling of unidirectional flow compartments and the thresholding of local alignment deformation f_f were modified with the goal of improving the accuracy of the compartment model RTD. Each unidirectional flow compartment was modelled as a series of CSTRs, and increasing the number of CSTRs from 1 to 3 in each series was observed to improve the resulting RTD by biasing the compartment model toward PFR-like behaviour. This decreased the variance ($\sigma^2 = 61.3\,\mathrm{s}^2$ to $39.8\,\mathrm{s}^2$) and skewness ($s^3 = 28.6\,\mathrm{s}^3$ to $24.3\,\mathrm{s}^3$) of the compartment model RTD towards the values of the continuum simulation, but did not significantly change the mean residence time t_m, so a large deviation from the continuum solution RTD remained. Increasing the number of CSTRs further resulted in greater deviation from the continuum solution variance and skewness. The lower threshold level of f_f was increased from 1 to 10, but this was not observed to have a significant impact on the compartment model RTD. RTDs for the compartment model were computed 400-900 times faster than the RTD for the continuum solution, confirming a major reduction in computational cost for the model.

7.2 Future Work

A major problem with current compartment modelling approaches is the lack of standardization of how the compartments are determined, also known as compartmentalization. The choice of variables to use for this determination is left to the user, as are the methods by which the range of these variables will be thresholded to differentiate separate compartments. The potential application of compartment modelling to reduce simulation costs motivates the development of a standardized approach to compartment modelling based on universal flow quantities.

The contribution of this work focuses on proposing novel, topologically-informed quantities for compartmentalization. These quantities are splay, twist, and bend, as well as the summation of these quantities, referred to as local alignment deformation. In this work, local alignment deformation is computed by equally weighing splay, twist, and bend. Future work could modify the computation of local alignment deformation by adjusting the coefficients k_{ii} to weigh splay, twist, and bend differently. These adjustments could be made by a traditional experimental design or automated by the application of artificial intelligence, with the goal of improving the quality of the compartment model based on RTD or some other measure.

Other areas of compartment modelling can be further developed:

- **Thresholding of Variables**: In this work, thresholding of the local alignment deformation is done manually. Future works could focus on developing standard thresholding approaches for compartment modelling. These approaches could be based on standard image processing methods for segmentation, such as those based on histogram analysis [39].
- **Hydrodynamic Approximations of Compartments**: Previous compartment modelling studies appear to exclusively approximate compartments as well-mixed. This approximation is not accurate for compartments that are dominated by unidirectional flow. The topological quantities proposed for compartmentalization in this work are able to identify distinct flow modes. Therefore, these quantities can be used to classify compartments and develop a compartment model with appropriate hydrodynamic approximations for each compartment (e.g. well-mixed, CSTRs-in-series, plug flow, etc). Laminar flow reactor models [2] are a promising candidate to approximate the hydrodynamics of compartments dominated by a unidirectional parabolic flow profile, which was not explored in this work.
- **Iteration between Compartment and Continuum Modelling**: For simulating multiphysics processes with coupled transport phenomena over very long timescales, it is necessary to iterate between continuum and compartment models. This is done to recalculate the flow field, which may be significantly altered by slower transport phenomena over a long enough period. Decisions about when to iterate between models are not considered in this work, and are another area of compartment modelling that is not rigorously justified.

References

[1] Elina K. Nauha, Zbyněk Kálal, Jama Mohamed Ali, and Ville Alopaeus. Compartmental modeling of large stirred tank bioreactors with high gas volume fractions. *Chemical Engineering Journal*, 334:2319–2334, February 2018.

[2] H Scott Fogler. *Elements of chemical reaction engineering*. Prentice Hall, 2016.

[3] Stelios Rigopoulos and Alan Jones. A hybrid CFD—reaction engineering framework for multiphase reactor modelling: basic concept and application to bubble column reactors. *Chemical Engineering Science*, 58(14):3077–3089, July 2003.

[4] Jérémie Haag, Caroline Gentric, Cécile Lemaitre, and Jean-Pierre Leclerc. Modelling of Chemical Reactors: From Systemic Approach to Compartmental Modelling. *International Journal of Chemical Reactor Engineering*, 16(8), 2018.

[5] Rajesh K Singh, Chao Wang, and Zhijie Xu. Residence time distribution in a structured packing unit for monitoring aerosol emissions. *International Journal of Greenhouse Gas Control*, 79:181–192, 2018.

[6] Jamshid Behin and S Bahrami. Modeling an industrial dissolved air flotation tank used for separating oil from wastewater. *Chemical Engineering and Processing: Process Intensification*, 59:1–8, 2012.

[7] LEAP CFD Team. Ansys cfd assists the pharmaceutical industry to address scale-up challenges. https://www.computationalfluiddynamics.com.au/ansys-cfd-assists-the-pharmaceutical-industry-to-address-scale-up-challenges/, 2016. Accessed: 2019-06-07.

[8] Markus Gresch, Raphael Brügger, Alain Meyer, and Willi Gujer. Compartmental Models for Continuous Flow Reactors Derived from CFD Simulations. *Environmental Science & Technology*, 43(7):2381–2387, April 2009.

[9] H. J. M. Kramer, J. W. Dijkstra, A. M. Neumann, R. ÓMeadhra, and G. M. van Rosmalen. Modelling of industrial crystallizers, a compartmental approach using a dynamic flow-sheeting tool. *Journal of Crystal Growth*, 166(1):1084–1088, September 1996.

[10] Sean K. Bermingham, Herman J. M. Kramer, and Gerda M. van Rosmalen. Towards on-scale crystalliser design using compartmental models. *Computers & Chemical Engineering*, 22:S355–S362, March 1998.

[11] J. Alex, G. Kolisch, and K. Krause. Model structure identification for wastewater treatment simulation based on computational fluid dynamics. *Water Science and Technology*, 45(4-5):325–334, February 2002.

[12] A. H. Alexopoulos, D. Maggioris, and CCFD Kiparissides. CFD analysis of turbulence non-homogeneity in mixing vessels: A two-compartment model. *Chemical Engineering Science*, 57(10):1735–1752, 2002.

[13] F. Bezzo, S. Macchietto, and C. C. Pantelides. General hybrid multizonal/CFD approach for bioreactor modeling. *AIChE Journal*, 49(8):2133–2148, 2003.

[14] F. Bezzo, S. Macchietto, and C. C. Pantelides. A general methodology for hybrid multizonal/CFD models: Part I. Theoretical framework. *Computers & Chemical Engineering*, 28(4):501–511, April 2004.

[15] F. Bezzo and S. Macchietto. A general methodology for hybrid multizonal/CFD models: Part II. Automatic zoning. *Computers & Chemical Engineering*, 28(4):513–525, April 2004.

[16] Tannaz Tajsoleiman, Robert Spann, Christian Bach, Krist V. Gernaey, Jakob Kjøbsted Huusom, and Ulrich Krühne. A CFD based automatic method for compartment model development. *Computers & Chemical Engineering*, 123(Complete):236–245, 2019.

[17] Anders Nørregaard, Christian Bach, Ulrich Krühne, Ulrik Borgbjerg, and Krist V. Gernaey. Hypothesis-driven compartment model for stirred bioreactors utilizing computational fluid dynamics and multiple pH sensors. *Chemical Engineering Journal*, 356(Complete):161–169, 2019.

[18] Angélique Delafosse, Marie-Laure Collignon, Sébastien Calvo, Frank Delvigne, Michel Crine, Philippe Thonart, and Dominique Toye. CFD-based compartment model for

description of mixing in bioreactors. *Chemical Engineering Science*, 106:76–85, March 2014.

[19] Marko Laakkonen. *Development and validation of mass transfer models for the design of agitated gas-liquid reactors*. Helsinki University of Technology, November 2006.

[20] Merve Öner, Christian Bach, Tannaz Tajsoleiman, Getachew S. Molla, Michael F. Freitag, Stuart M. Stocks, Jens Abildskov, Ulrich Krühne, and Gürkan Sin. Scale-up Modeling of a Pharmaceutical Crystallization Process via Compartmentalization Approach. In *Computer Aided Chemical Engineering*, volume 44, pages 181–186. Elsevier, 2018.

[21] E. Kougoulos, A. G. Jones, and M. W. Wood-Kaczmar. A hybrid CFD compartmentalization modeling framework for the scaleup of batch cooling crystallization processes. *Chemical Engineering Communications*, 193(8):1008–1023, 2006.

[22] Xi Yu, Michael J. Hounslow, Gavin K. Reynolds, Anders Rasmuson, Ingela Niklasson Björn, and Per J. Abrahamsson. A compartmental CFD-PBM model of high shear wet granulation. *AIChE Journal*, 63(2):438–458, 2017.

[23] Gary J. Wells and W. Harmon Ray. Methodology for modeling detailed imperfect mixing effects in complex reactors. *AIChE Journal*, 51(5):1508–1520, 2005.

[24] Y. Le Moullec, C. Gentric, O. Potier, and J. P. Leclerc. Comparison of systemic, compartmental and CFD modelling approaches: Application to the simulation of a biological reactor of wastewater treatment. *Chemical Engineering Science*, 65(1):343–350, January 2010.

[25] Elina K. Nauha and Ville Alopaeus. Modeling method for combining fluid dynamics and algal growth in a bubble column photobioreactor. *Chemical Engineering Journal*, 229:559–568, August 2013.

[26] Andres Alvarado, Sreepriya Vedantam, Peter Goethals, and Ingmar Nopens. A compartmental model to describe hydraulics in a full-scale waste stabilization pond. *Water Research*, 46(2):521–530, February 2012.

[27] Rory FD Monaghan and Ahmed F Ghoniem. A dynamic reduced order model for simulating entrained flow gasifiers: Part i: Model development and description. *Fuel*, 91(1):61–80, 2012.

[28] Matteo Gazzani, Giampaolo Manzolini, Ennio Macchi, and Ahmed F Ghoniem. Reduced order modeling of the shell–prenflo entrained flow gasifier. *Fuel*, 104:822–837, 2013.

[29] M Hossein Sahraei, Marc A Duchesne, Robert Yandon, Adrian Majeski, Robin W Hughes, and Luis A Ricardez-Sandoval. Reduced order modeling of a short-residence time gasifier. *Fuel*, 161:222–232, 2015.

[30] M Hossein Sahraei, Marc A Duchesne, Robin W Hughes, and Luis A Ricardez-Sandoval. Dynamic reduced order modeling of an entrained-flow slagging gasifier using a new recirculation ratio correlation. *Fuel*, 196:520–531, 2017.

[31] Tony McLoughlin, Robert S. Laramee, Ronald Peikert, Frits H. Post, and Min Chen. Over two decades of integration-based, geometric flow visualization. *Computer Graphics Forum*, 29(6):1807–1829, 2010.

[32] Vivek Verma, David Kao, and Alex Pang. A flow-guided streamline seeding strategy. In *Proceedings of the Conference on Visualization '00*, VIS '00, pages 163–170, Los Alamitos, CA, USA, 2000. IEEE Computer Society Press.

[33] R. Byron Bird, Warren E. Stewart, and Edwin N. Lightfoot. *Transport Phenomena*. John Wiley & Sons, Inc., 2nd revised edition, 2007.

[34] J R Kelly and P Palffy-Muhoray. The optical response of polymer dispersed liquid crystals. *Molecular Crystals and Liquid Crystals*, 243(3):11–29, 1994.

[35] F. C. Frank. I. Liquid crystals. On the theory of liquid crystals. *Discussions of the Faraday Society*, 25:19, 1958.

[36] Robert H. Chen. *Liquid crystal displays*. Wiley, 2011.

[37] William B Krantz. *Scaling analysis in modeling transport and reaction processes: a systematic approach to model building and the art of approximation*. Wiley. com, 2007.

[38] The OpenFOAM Foundation. *`OpenFOAM` Programmer's Guide*, 2014.

[39] Wilhelm Burger and Mark J Burge. *Principles of Digital Image Processing: Advanced Methods*. Springer Science & Business Media, 2013.

[40] Utkarsh Ayachit. The paraview guide. *Kitware Inc.: New York, NY, USA*, page 237, 2016.

[41] Bahram Haddadi, Clemens Gößnitzer, Sylvia Zibuschka, and Yitong Chen. Openfoam basic training tutorial ten residence time distribution, 09 2019.

[42] Eric Jones, Travis Oliphant, Pearu Peterson, et al. SciPy: Open source scientific tools for Python, 2001.